J. Fluid Mech. (2022), *vol*. 936, A18, doi:10.1017/jfm.2022.53

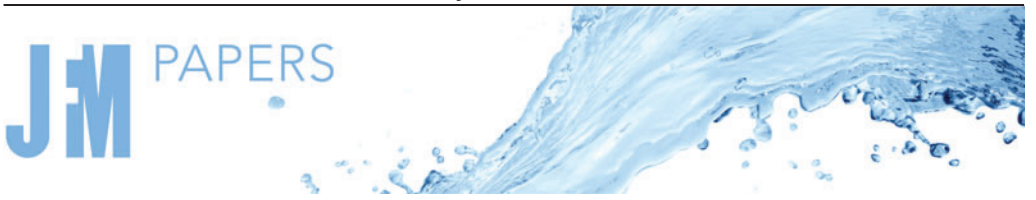

Reflection of rightward moving shocks of the first and second families over a steady oblique shock wave

Miao-Miao Wang[1] **and Zi-Niu Wu**[1],†

[1]Department of Engineering Mechanics, Tsinghua University, Beijing 100084, PR China

(Received 29 July 2021; revised 30 November 2021; accepted 15 January 2022)

The reflection of rightward moving shocks (RMSs) belonging to the first and second families, over an initially steady oblique shock wave (SOSW) produced by a wedge, is studied in this paper. Various possible combinations of primary reflection (reflection at the intersection point of the RMS and the SOSW) and secondary reflection (reflection, on the wedge, of reflected shock waves of the primary reflection) are identified and the transition conditions are studied. For an RMS of the first family, the shock reflection problem can be shown to be equivalent to a shock interference problem. If the wedge angle is large, then the problem is equivalent to a shock interaction problem with two incident shock waves of the same family so that we have type VI, type V and type IV shock interferences. Interestingly, when the wedge angle is small enough, deflection angle reversal is observed for the SOSW so that the right part of the SOSW can no longer be regarded as one incident shock wave. It is now the left part of the SOSW that becomes one incident shock wave. As a result, for a small wedge angle, type I or type II shock interference is observed. If the RMS belongs to the second family, then the primary reflection may have regular and Mach reflections, and one reflected shock of this primary reflection reflects over the wall as another pseudo-steady shock reflection, while the other reflected shock wave may be smooth or have a kink or a triple point, as in single, transitional and double Mach reflection of pseudo-steady shock reflection.

Key words: high-speed flow, shock waves

1. Introduction

Shock reflection is an important phenomenon in high-speed flow and is divided into steady reflection, pseudo-steady reflection and unsteady reflection by Ben-Dor (1988), who also documented the related knowledge in a monograph (Ben-Dor 2007).

† Email address for correspondence: ziniuwu@tsinghua.edu.cn

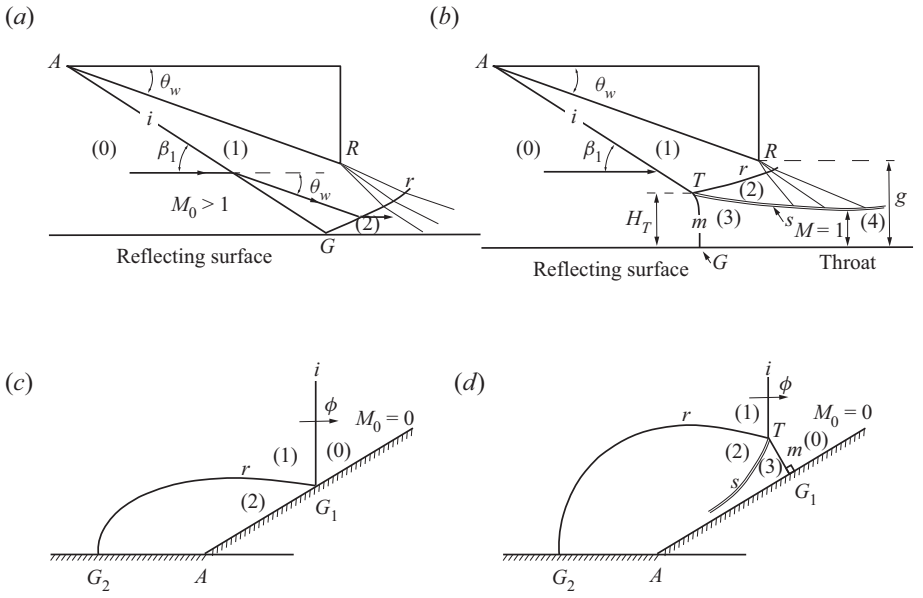

Figure 1. Illustration of shock reflection in supersonic flow: (*a*) steady symmetric RR, (*b*) steady symmetric MR, (*c*) pseudo-steady RR, (*d*) pseudo-steady MR.

Steady shock reflection occurs when an incident oblique shock wave caused by a wedge of wedge angle θ_w in a supersonic flow with upstream Mach number M_0 reflects over a reflecting surface. Both regular reflection (RR) as shown in figure 1(*a*), and Mach reflection (MR) as shown in figure 1(*b*), exist depending on the conditions of inflow Mach number and wedge angle. The transition condition between RR and MR has been extensively studied since the work of von Neumann (1943, 1945). There are two transition criteria: the von Neumann condition, which is the necessary condition for Mach reflection, and the detachment condition, which is the sufficient condition for Mach reflection to occur. In the M_0–θ_w plane, these two conditions divide the space into a regular reflection region where only regular reflection can occur, a Mach reflection region where only Mach reflection can occur, and a dual solution domain (DSD) where both regular reflection and Mach reflection are possible (Henderson & Lozzi 1975; Hornung, Oertel & Sandeman 1979; Teshukov 1989; Li & Ben-Dor 1996). A wedge-angle variation-induced hysteresis was proposed by Hornung *et al.* (1979) and later proved by Chpoun *et al.* (1995) using experimental study and Vuillon, Zeitoun & Ben-Dor (1995) using numerical simulation, and a Mach number variation-induced hysteresis was demonstrated by Ivanov *et al.* (2001). According to this hysteresis study, whether we have Mach reflection or regular reflection in the dual solution domain depends on the history of the building of the actual steady flow (Ben-Dor *et al.* 2002; Hornung 2014). In steady asymmetric shock reflection, where two incident shock waves are from the opposite wedges of different geometry, it is possible to have indirect Mach reflection (InMR), compared to the usual direct Mach reflection (DiMR). Li, Chpoun & Ben-Dor (1999) and Ivanov *et al.* (2002) clarified the domains of RR, MR and DSD, together with the regions to have DiMR or InMR for each triple point.

Pseudo-steady shock reflection happens when a planar incident shock wave moving with a constant velocity encounters a sharp compressive straight wedge immersed initially in a still gas. Both regular and irregular reflections may occur, depending on the

incident shock wave Mach number M_s, defined as the ratio between the shock speed ϕ and the sound speed a_0 in the still gas, and the reflecting wedge angle θ_w. Regular reflection is displayed schematically in figure 1(*c*). There are, however, numerous types of irregular reflections, including basically the von Neumann reflection, also called weak Mach reflection or Guderley reflection (see § 3.3 of Ben-Dor 2006), and Mach reflection in the usual sense. Mach reflection is further subdivided into single Mach reflection (SMR), transitional Mach reflection (TMR) and double Mach reflection (DMR). Figure 1(*d*) shows only the single Mach reflection case. For details of various types of Mach reflection and their transition criteria, see the review of Ben-Dor (2006). Semenov, Berezkina & Krassovskaya (2012) provided a slightly different classification of the Mach reflection.

There are possible applications in which the moving incident shock wave encounters a body immersed initially in a supersonic flow. In this case, there is a steady oblique shock wave (SOSW) ahead of the body before the moving incident shock wave impinges the wedge through reflecting over its oblique shock wave, if the reference frame is attached to the body. This is the problem of reflection of a rightward moving shock (RMS) over an SOSW considered in this paper.

This situation may occur when a supersonic or hypersonic vehicle encounters the shock wave of an upstream vehicle moving more slowly; the shock wave of the latter may reflect over the shock wave of the former (Klopfer, Yee & Kutler 1989). Another situation arises from the disturbance in the form of an upstream shock wave that enters into a supersonic inlet with oblique shock waves inside this inlet. Kudryavtsev *et al.* (2002) studied such a case and showed that such a disturbance may force transition from regular reflection to Mach reflection of the oblique shock wave inside the inlet. More generally, the reflection of a moving shock wave over another shock wave has been studied before within the context of shock-on-shock interaction (Kutler, Sakell & Aiello 1975; Li & Ben-Dor 1997; Law, Felthun & Skews 2003; Smyrl 2006). Li & Ben-Dor (1997) illustrated the two possible problems with such interaction: one is in interception of a supersonic vehicle with a blast wave, and the other is in the encounter between two supersonic vehicles travelling in opposite directions.

However, past studies about reflection of an RMS over an SOSW, or equivalently shock-on-shock interaction, appeared to be restricted to the problem where the RMS belongs to the second family, i.e. the flow stream is towards the left-hand side in the frame co-moving with the RMS. The problem where the RMS is of the first family, for which the flow stream is towards the right-hand side in the frame co-moving with the RMS, is also important. One such example is the encounter of a supersonic projectile overtaking the bow shock wave formed initially at the exit of a launched tube, studied experimentally by Athira *et al.* (2020). It is thus interesting to study the difference between shock reflection patterns for RMSs of the first and second families, and this forms the objective of the present paper. It is expected that RMSs of the first and second families may cause different reflection patterns.

The aim of this paper is to identify, through numerical simulation and transition condition analysis, the possible shock reflection types for each family and the transition conditions. We will examine the similarity of the present problem with the classical Edney steady shock interaction (Edney 1968), since using a properly chosen reference frame means that the problem can be made equivalent to Edney's problem. Recall that, depending on the location of interaction and the strength of the shock waves near the interaction points, there are six types of shock/shock interferences (Edney 1968; Bramlette 1974; Frame & Lewis 1997; Grasso, Purpura & Délery 2003; Windisch, Reinartz & Muler

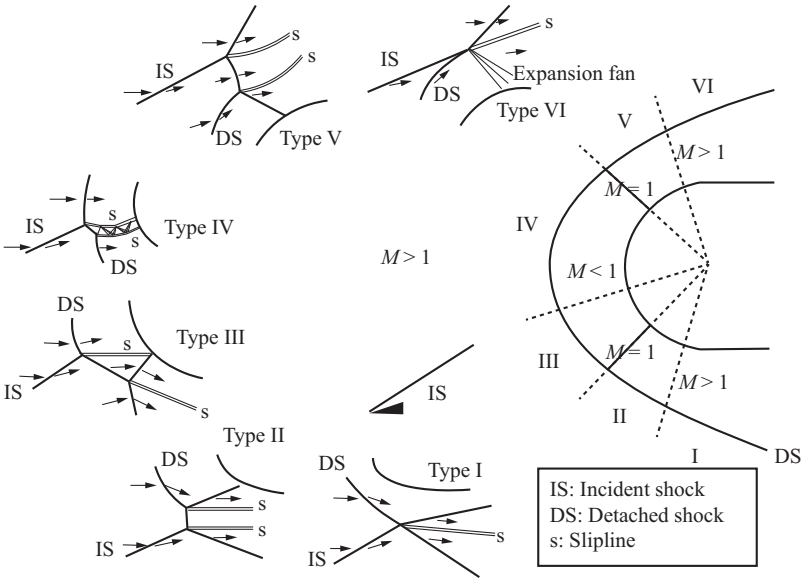

Figure 2. Illustration of Edney's six types of shock interaction.

2016); their flow patterns and the situations to produce them are illustrated in figure 2. It is also interesting to examine whether the present reflection shares some similarity with the classical pseudo-steady shock reflection problem shown in figures 1(*c*,*d*).The rest of this paper will be organized as follows.

The problem that we consider will be defined in § 2, where we also provide the necessary shock relations, some properties of RMSs of both families, and the numerical methods used in this paper.

In § 3, we will study shock reflection for an RMS of the first family. The transition condition is studied by switching the present problem to an equivalent steady shock interaction problem where typically type I to type VI shock interferences are basic flow patterns. Numerical simulation will be used to display the possible shock reflection patterns. In this section, a flow deflection angle reversal will be observed, and its significance in changing the role of incident shock waves and the reflection type is discussed.

In § 4, we will study shock reflection for an RMS of the second family. The transition condition is studied using a reference frame co-moving with the intersection point of the RMS and the SOSW. Numerical simulation will be used to display the possible shock reflection patterns. The global reflection pattern is subdivided into primary reflection (reflection at the intersection point of the RMS and the SOSW) and secondary reflection (reflection of the reflected shock from primary reflection). This not only allows us to go into details of the primary reflection patterns, but also reveals some phenomena related to secondary reflection.

Conclusions will be stated in § 5.

In this paper, we use ρ, p, u, v, a, M and γ to denote the density, pressure, the two components of flow velocity, sound speed, Mach number and ratio of specific heats, respectively. The sound speed is computed as $a = \sqrt{\gamma p/\rho}$.

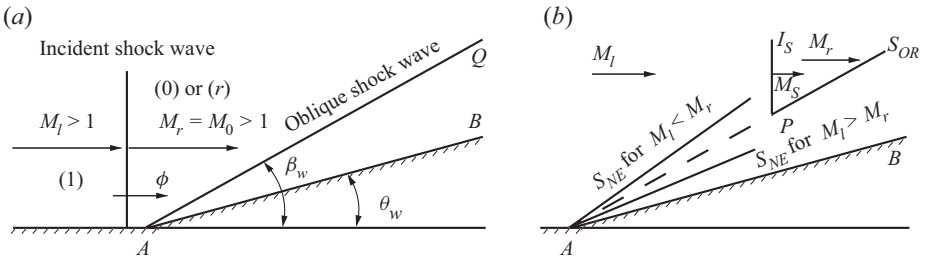

Figure 3. Reflection between a right-going incident shock wave and an SOSW attached to a sharp wedge: (*a*) initial state; (*b*) a typical moment.

2. Problem definition, shock relations and numerical method

This section defines the shock reflection problem where the RMS may belong to the first and second families, provides the shock relations for both moving and steady-state shock waves, discusses some properties of the RMS, and gives the numerical method used and the method to identify a triple point structure.

2.1. *Definition of the present shock reflection problem*

The shock reflection problem that we consider is displayed schematically in figure 3(*a*). A wedge of angle θ_w is immersed in an initially steady supersonic flow with Mach number M_0 and produces an SOSW with shock angle β_w. A rightward moving normal shock starting at the inlet and moving at constant speed ϕ impinges the oblique shock wave to produce a shock reflection between a moving shock wave and an oblique shock.

The left status of this RMS will be denoted with subscript l, and the flow parameters in region (0) will be denoted with subscript r. In this paper we consider only the case where $M_l > 1$, i.e. the inlet remains supersonic behind the RMS. The speed of the shock may also be measured with the shock moving Mach number $M_s = \phi/a_r$, where a_r is the sound speed in region (0).

As shown in figure 3(*b*), that part of the RMS above the intersection point P of the RMS and the SOSW will be denoted shock I_S, meaning the incident shock wave. At reflection, the unperturbed part of the SOSW (downstream of P) will be denoted shock S_{OR}, with the subscript OR meaning the original SOSW. The oblique shock wave newly created with new inflow condition updated by the RMS will be denoted S_{NE}.

Both first and second families are considered for the RMS. For an RMS of the first family, one has $p_r > p_l$, and in the frame co-moving with the RMS, the flow stream is towards the right-hand side. For an RMS of the second family, one has $p_r < p_l$, and in the frame co-moving with the RMS, the flow stream is towards the left-hand side. Reflection with an RMS of the first family may occur when one supersonic object penetrates the shock wave of another supersonic object that has a smaller speed and is upstream initially. Reflection with an RMS of the second family may occur when two supersonic objects move in the opposite direction, with one penetrating the shock wave of another. In this paper, we consider only the case that the penetrating object (here simplified as a wedge) penetrates perpendicularly to the shock wave of the other.

We will work with a reference frame co-moving with the intersection point P. It is obvious that the intersection point P has velocity

$$V_P = (u_P, v_P) = (M_s a_r, M_s a_r \tan\beta_w), \tag{2.1}$$

where β_w is the shock angle of the undisturbed (original) SOSW.

In the following, we will need repeatedly the oblique shock wave relations, which will, for brevity, be abbreviated as

$$M_d^2 = f_M(M_u, \beta_{ud}), \quad p_d = p_u f_p(M_u, \beta_{ud}), \quad \rho_d = \rho_u f_\rho(M_u, \beta_{ud}), \tag{2.2a–c}$$

where

$$\left.\begin{aligned} f_M(M,\beta) &= \frac{M^2 + \dfrac{2}{\gamma-1}}{\dfrac{2\gamma}{\gamma-1}M^2\sin^2\beta - 1} + \frac{M^2\cos^2\beta}{\dfrac{\gamma-1}{2}M^2\sin^2\beta + 1}, \\ f_p(M,\beta) &= 1 + \frac{2\gamma}{\gamma+1}\left((M\sin\beta)^2 - 1\right), \\ f_\rho(M,\beta) &= \frac{(\gamma+1)(M\sin\beta)^2}{2 + (\gamma-1)(M\sin\beta)^2}. \end{aligned}\right\} \tag{2.3}$$

In (2.2a–c) and (2.3), the subscript u denotes the flow parameters upstream of the shock wave, and d downstream; β_{ud} is the shock angle that is related to the flow deflection angle θ_{ud} by the shock angle relation

$$\tan\theta_{ud} = f_\theta(M_u, \beta_{ud}), \quad f_\theta(M,\beta) = \frac{2\left(M^2\sin^2\beta - 1\right)}{\left(M^2(\gamma + \cos 2\beta) + 2\right)\tan\beta}. \tag{2.4a,b}$$

For a given upstream Mach number M_u and flow deflection angle θ_{ud}, there are two solutions for β_{ud}; the smaller one corresponds to a weak solution, and the larger one corresponds to a strong solution. There is a maximum value for the flow deflection angle $\theta = \theta^{(max)}(M_u)$, which is determined by $\partial f_\theta(M_u, \beta_{ud})/\partial\beta_{ud} = 0$. The expression for the detached angle is

$$\left.\begin{aligned} \sin^2\beta_m &= \frac{1}{\gamma M_u^2}\left[\frac{\gamma+1}{4}M_u^2 - 1 + \sqrt{(1+\gamma)\left(1 + \frac{\gamma-1}{2}M_u^2 + \frac{\gamma+1}{16}M_u^4\right)}\right], \\ \tan\theta^{(max)} &= \frac{2[(M_u^2-1)\tan^2\beta_m - 1]}{\tan\beta_m\left[(\gamma M_u^2 + 2)(1+\tan^2\beta_m) + M_u(1-\tan^2\beta_m)\right]}. \end{aligned}\right\} \tag{2.5}$$

For a given M_u, there is a flow deflection angle at which the downstream shock wave has sonic flow (i.e. $M_d = 1$), beyond which the shock is a strong shock (with $M_d < 1$), compared to weak shock (with $M_d > 1$) for a smaller flow deflection angle.

2.2. *Shock relations for RMSs of the first and second families*

For RMSs of both families, the flow parameters M_l, u_l, ρ_l, p_l on the left of an RMS can be related to the flow parameters M_r, u_r, ρ_r, p_r on the right of the RMS and the shock speed ϕ or the shock Mach number M_s.

For an RMS of the first family, $p_l < p_r$ and we have (Ben-Dor *et al.* 2001)

$$\phi = u_r - a_r\sqrt{\frac{\gamma+1}{2\gamma}\frac{p_l}{p_r}+\frac{\gamma-1}{2\gamma}} \tag{2.6}$$

and

$$u_l = u_r - \frac{a_r}{\gamma}\left(\frac{p_l}{p_r}-1\right)\left(\frac{\gamma+1}{2\gamma}\frac{p_l}{p_r}+\frac{\gamma-1}{2\gamma}\right)^{-1/2}. \tag{2.7}$$

For an RMS of the second family, $p_r < p_l$ and we have (Ben-Dor *et al.* 2001)

$$\phi = u_r + a_r\sqrt{\frac{\gamma+1}{2\gamma}\frac{p_l}{p_r}+\frac{\gamma-1}{2\gamma}} \tag{2.8}$$

and

$$u_r = u_l + \frac{a_l}{\gamma}\left(\frac{p_r}{p_l}-1\right)\left(\frac{\gamma+1}{2\gamma}\frac{p_r}{p_l}+\frac{\gamma-1}{2\gamma}\right)^{-1/2}. \tag{2.9}$$

Both (2.6) and (2.8) can be used to express the pressure ratio as a function of the Mach numbers M_r and M_s:

$$\frac{p_l}{p_r} = \psi, \tag{2.10}$$

where

$$\psi = \frac{2\gamma(M_r - M_s)^2 - (\gamma-1)}{\gamma+1}. \tag{2.11}$$

The shock relation for density and the sound speed expression can be used to give

$$\frac{\rho_l}{\rho_r} = \frac{1+\dfrac{\gamma+1}{\gamma-1}\psi}{\psi+\dfrac{\gamma+1}{\gamma-1}}, \quad \frac{a_l}{a_r} = \sqrt{\psi\,\frac{\psi+\dfrac{\gamma+1}{\gamma-1}}{1+\dfrac{\gamma+1}{\gamma-1}\psi}}. \tag{2.12a,b}$$

Insert (2.7) for u_l and (2.12a,b) for a_l into $M_l = u_l/a_l$, and using (2.10) to replace p_l/p_r by ψ, we get, for an RMS of the first family,

$$M_l = \frac{M_r - \dfrac{1}{\gamma}(\psi-1)\left(\dfrac{\gamma+1}{2\gamma}\psi+\dfrac{\gamma-1}{2\gamma}\right)^{-1/2}}{\sqrt{\psi\,\dfrac{\psi+\dfrac{\gamma+1}{\gamma-1}}{1+\dfrac{\gamma+1}{\gamma-1}\psi}}}. \tag{2.13}$$

Similarly, for an RMS of the second family, we have

$$M_l = \frac{\left(\dfrac{\gamma+1}{2}-\dfrac{M_s}{M_r}\right)\dfrac{1}{\psi}+\left(\dfrac{\gamma-1}{2}+\dfrac{M_s}{M_r}\right)}{\gamma\left(\dfrac{M_s}{M_r}-1\right)\sqrt{\dfrac{\gamma+1}{2\gamma}\dfrac{1}{\psi}+\dfrac{\gamma-1}{2\gamma}}}. \tag{2.14}$$

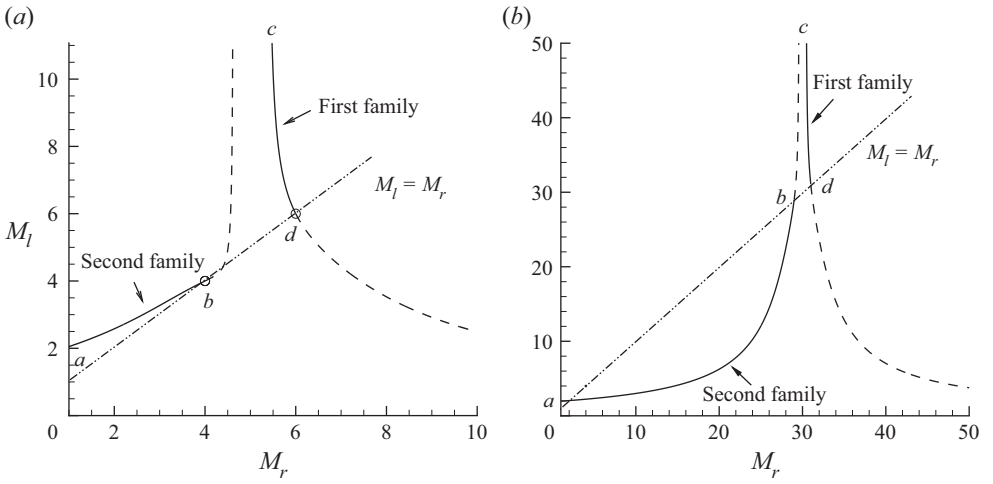

Figure 4. The Mach number M_l as a function of M_r: (*a*) $M_s = 5$; (*b*) $M_s = 30$.

2.3. *Properties of RMSs of both families*

Now we display how M_l and p_l/p_r vary with respect to M_r or M_s. The variation of the Mach number M_l with respect to M_r and M_s is computed by (2.13) and is displayed in figures 4(*a*) for $M_s = 5$ and 4(*b*) for $M_s = 30$.

For an RMS of the first family, $M_l \to \infty$ when $\psi = 0$, according to (2.13). By (2.11), $\psi = 0$ means $M_r = M_s + \sqrt{(\gamma - 1)/(2\gamma)}$. If $M_s = 5$, then $M_r = 5.378$, which is the abscissa of point c in figure 4(*a*). The value of M_l towards the point c is infinite. The condition $p_l = p_r$ occurs when $\psi = 1$. If $M_s = 5$, then $M_r = 6$, which is the abscissa of point d in figure 4(*a*). Thus M_r has a finite range of values for an RMS of the first family, and we have $5.378 < M_r < 6$ for $M_s = 5$. If $M_s = 30$, then $M_r = 30.378$, which is the abscissa of point c in figure 4(*b*). The value of M_l towards the point c is infinite. The condition $p_l = p_r$ occurs when $\psi = 1$. If $M_s = 30$, then $M_r = 31$, which is the abscissa of point d in figure 4(*b*). Thus M_r has a finite range of values for an RMS of the first family, and we have $30.378 < M_r < 31$ for $M_s = 30$.

For an RMS of the second family, M_r also has a finite range of values. The point a in figure 4(*a*) corresponds to $M_r = 1$, at which $M_l = 2.05$ according to (2.14). The point b corresponds to $p_l = p_r$, i.e. $\psi = 1$. With $\psi = 1$, (2.11) gives $M_r = M_s - 1 = 4$ for $M_s = 5$. The point a in figure 4(*b*) corresponds to $M_r = 1$, at which $M_l = 1.96$ according to (2.14). The point b corresponds to $p_l = p_r$, i.e. $\psi = 1$. With $\psi = 1$, (2.11) gives $M_r = M_s - 1 = 29$ for $M_s = 30$.

In figure 5(*a*), the variance of M_l with the change of M_s for $M_r = 6$ is displayed. For an RMS of the first family, $M_l \to \infty$ when $\psi = 0$, according to (2.13). By (2.11), $\psi = 0$ means $M_s = M_r - \sqrt{(\gamma - 1)/(2\gamma)}$. If $M_r = 6$, then $M_s = 5.622$, which is the abscissa of point b in figure 5(*a*). The value of M_l towards the point b is infinite. The condition $p_l = p_r$ occurs when $\psi = 1$. If $M_r = 6$, then (2.11) gives $M_s = 5$, which is the abscissa of point a in figure 5(*a*). Thus M_s has a finite range of values for an RMS of the first family, and we have $5 < M_s < 5.622$ for $M_r = 6$. For an RMS of the second family, the point d in figure 4(*a*) corresponds to $M_s = 30$, at which $M_l = 2.443$ according to (2.14). The point c corresponds to $p_l = p_r$, i.e. $\psi = 1$. With $\psi = 1$, (2.11) gives $M_s = M_r + 1 = 7$ for $M_r = 6$.

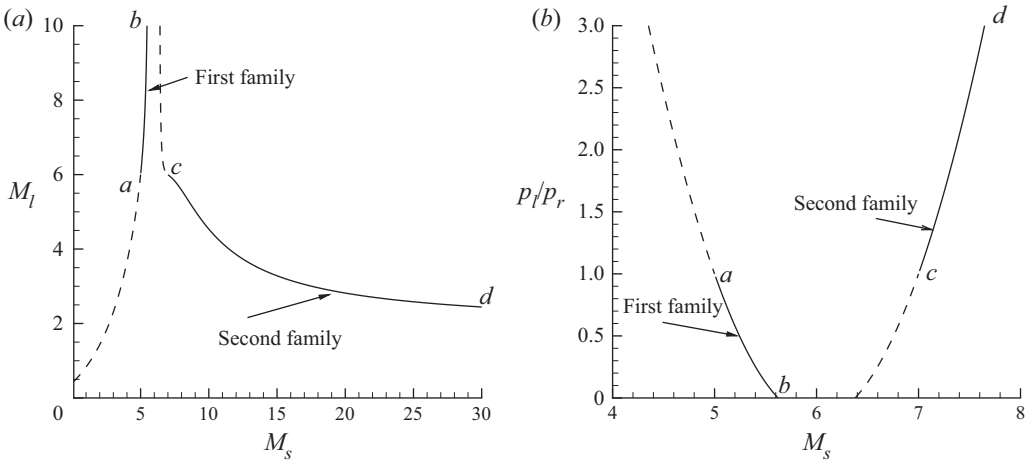

Figure 5. (*a*) The Mach number M_l as a function of M_s with $M_r = 6$; (*b*) p_l/p_r as a function of M_s with $M_r = 6$.

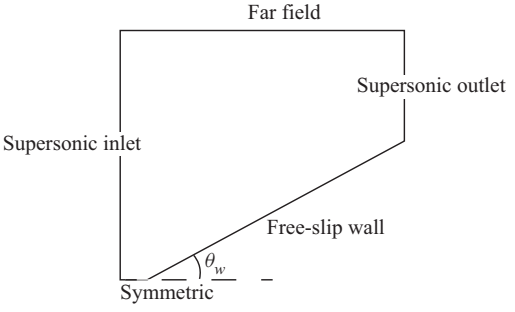

Figure 6. Domain of computation and boundary condition for the numerical simulation.

In figure 5(*b*), the variance of p_l/p_r (or ψ) with the change of M_s for $M_r = 6$ is displayed. For an RMS of the first family, by (2.11), $\psi = 0$ means $M_s = M_r - \sqrt{(\gamma - 1)/(2\gamma)}$. If $M_r = 6$, then $M_s = 5.622$, which is the abscissa of point b in figure 5(*b*). The condition $p_l = p_r$ occurs when $\psi = 1$. If $M_r = 6$, then (2.11) gives $M_s = M_r - 1 = 5$, which is the abscissa of point a in figure 5(*b*). Thus M_s has a finite range of values for an RMS of the first family, and we have $5 < M_s < 5.622$ for $M_r = 6$. For an RMS of the second family, the point d in figure 5(*b*) corresponds to $M_s = 7.648$, at which M_l =5.761 according to (2.14). The point c corresponds to $p_l = p_r$, i.e. $\psi = 1$. With $\psi = 1$, (2.11) gives $M_s = M_r + 1 = 7$ for $M_r = 6$.

2.4. *Numerical method*

Computational fluid dynamics (CFD) will be used to display shock reflection patterns for specific input conditions. The compressible Euler equations of an ideal gas are solved using the second-order implicit advection upstream splitting method (AUSM) (Liu 1996). The computational domain and the boundary conditions are shown in figure 6. The lower boundary is a wedge with wedge angle θ_w.

First we compute a steady supersonic flow with inflow Mach number M_0. This will give a simple supersonic flow with an oblique shock wave with shock angle β_w.

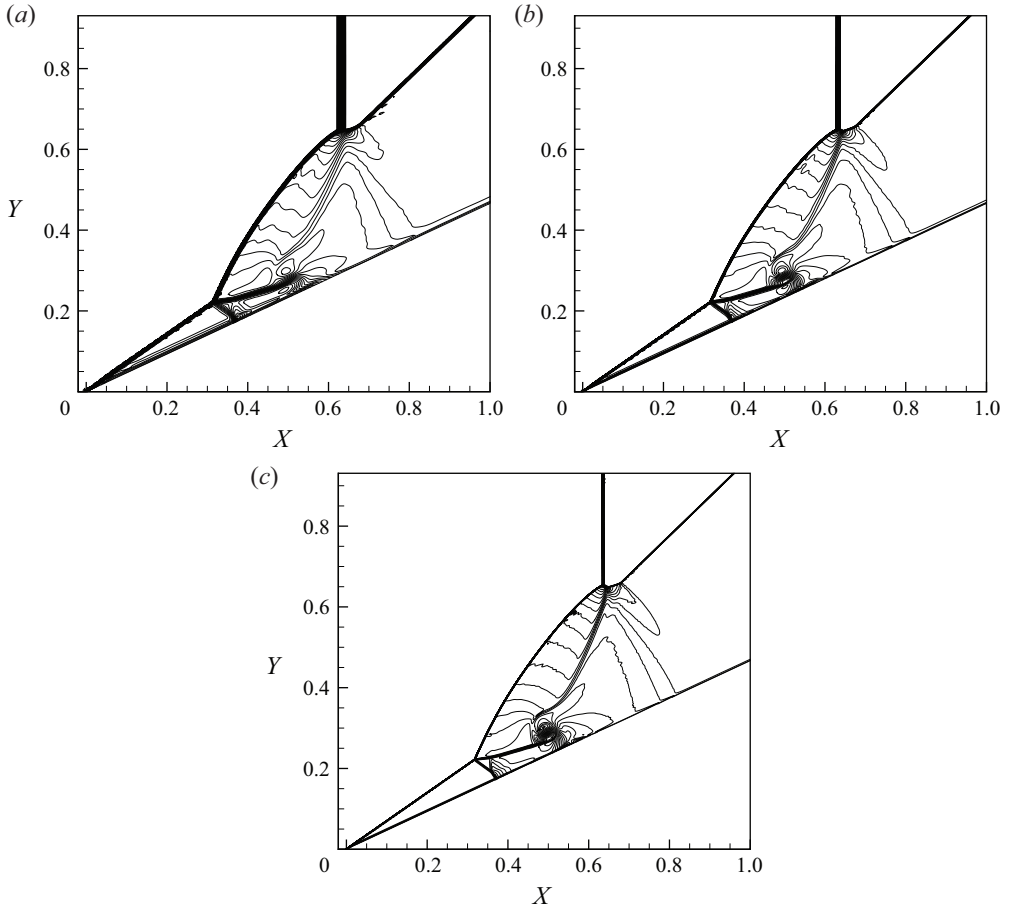

Figure 7. Mach contours with different meshes: (*a*) 250 × 250 cells, (*b*) 500 × 500 cells, (*c*) 1000 × 1000 cells.

Then, at the inlet upstream of the wedge, we set an RMS moving at a given M_s. The original steady-state solutions are now considered as the right-hand state of this RMS. The left-hand side flow parameters M_l, p_l and ρ_l of this RMS are obtained from the expressions (2.10)–(2.13).

To test the accuracy with a different choice of grid density, we consider an RMS of the first family with $\theta_w = 25^\circ$, $M_s = 2.45$ and $M_r = 3$. Three grids are tested. The coarser grid has 250 × 250 cells, the middle grid has 500 × 500 cells, and the finest grid has 1000 × 1000 cells. The Mach contours at the same typical instant are displayed in figure 7 for the three grids. The shock wave patterns calculated with the middle and finest grids have little difference, as shown in figure 7, so the finest grid is used for the subsequent numerical simulations.

2.5. *Solution and identification of steady and moving triple points*

The problem studied in this paper may display a shock reflection configuration with several moving triple points. The typical flow structure for a triple point configuration is shown in figure 8, where we distinguish between an upward triple point and a downward

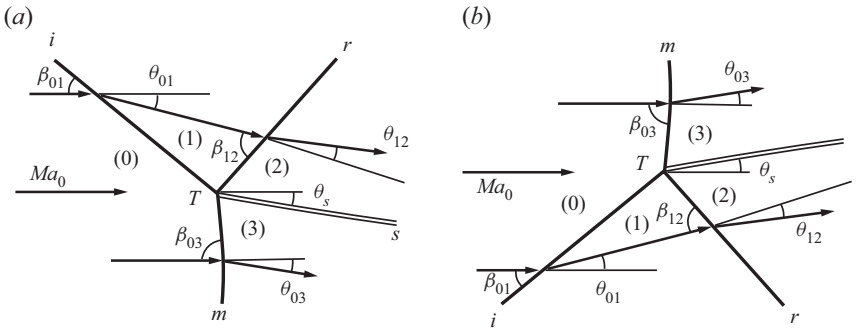

Figure 8. A triple point structure: (*a*) upward triple point; (*b*) downward triple point.

triple point. It involves an incident shock (labelled *i*), a reflected shock (labelled *r*), a Mach stem (labelled *m*) and a slipline (labelled *s*). The flow in the vicinity of a steady triple point is determined by the von Neumann triple point theory: the flow properties in the adjacent regions (regions (0)–(3) in figure 8) are connected by oblique shock wave relations with an assumed slipline angle θ_s, and this slipline angle is finally determined by the pressure balance condition ($p_3 = p_2$) and flow parallel condition ($\theta_{03} = \theta_s$, $\theta_{02} = \theta_{01} - \theta_s$). The pressure balance condition states that the pressure behind the reflected shock wave is balanced with that behind the Mach stem; the flow parallel condition states that the flow streams across the slipline are parallel.

In the following, we need an efficient method to identify a moving triple point structure through numerical solution of unsteady flow, i.e. to identify which of the shock waves of a triple point are the incident one, the reflected one and the Mach stem, from numerical solutions. For this, we will use the triple point structure identification (TPSI) method of Wang & Wu (2021); see the Appendix for how to use it.

3. Reflection types and transition conditions for an RMS of the first family

In this section, we first display one shock reflection pattern and make a transformation to show that this reflection pattern can be related to type V shock interaction, and suggest that the present shock reflection problem with an RMS of the first family (called the original problem below) can be reduced to an equivalent shock interference problem (called the equivalent problem below), i.e. the shock interference problem of Edney (1968) or shock interaction with double wedge geometry (Olejniczak, Wright & Candler 1997), which produce, for instance, type VI, V, IV shock interferences. A link is thus established between the input parameters of the original problem and the input parameters of the equivalent problem. Using this link, possible shock reflection patterns and transition conditions are discussed. A flow deflection angle reversal is observed, which alters the role of shock S_{OR} and shock S_{NE}, so that type I and type II shock interactions also occur.

3.1. *A shock reflection pattern that can be interpreted as type V shock interference*

We compute here an initially steady supersonic flow with $M_0 = 6$ and $\theta_w = 30^\circ$. This will give an SOSW. Then, at the inlet, we set an RMS of the first family moving at $M_s = 5.498$. The original flow parameters in region (0) are now considered as the right-hand state of this RMS. The left-hand side flow parameters of this RMS are set to $M_l = 10.889$

(obtained from (2.13) for the first family), $p_l = 0.127p_r$ and $\rho_l = 0.288\rho_r$ (obtained from (2.10)–(2.12*a*,*b*)).

The Mach contours at some typical instant where the major reflection structure is well formed are displayed in figure 9(*a*). The shock reflection pattern, with typical triple point structure illustrated, is displayed in figure 9(*b*). The shock reflection pattern displayed in figure 9(*b*) has five triple points (labelled Tp_1, Tp_2, Tp_3, Tp_4, Tp_5), identified using the TPSI method given in Appendix. The incident shock, reflected shock, Mach stem and slipline are marked with i, r, m and S, with subscripts 1, 2, 3, 4, 5 for the corresponding triple points. For instance, i_1, r_1, m_1, S_1 mark, respectively, the incident shock, reflected shock, Mach stem and slipline of triple point Tp_1. Note that this flow structure is similar to the reflection pattern of that given by Wang & Wu (2021) using $M_0 = 6$, $\theta_w = 22.5^\circ$ and $M_s = 5.58$. This similarity means that the five triple points structure may occur at close but different conditions. The schematic display in figure 9(*b*) has more details than that of Wang & Wu (2021): we display here streamlines for each triple (these streamlines are based on the flow relative to the frame co-moving with that triple point). The direction of a streamline indicates how pressure changes across any shock wave. The pressure downstream of a shock is larger than that upstream. Consider, for instance, triple point Tp_3. For an RMS of the first family, $p_l < p_r$ according to figure 5(*b*), thus one streamline relative to triple point Tp_3 points from region (r) to region (l) when crossing the RMS (shock 'I_s' in figure 9*b*) of figure 3(*a*).

The five triple points structure displayed in figure 9(*b*) is in fact a type V shock interference, which occurs in Edney's shock interaction problem (Edney 1968) and in the double wedge shock reflection problem (cf. Olejniczak *et al.* 1997; Hu *et al.* 2010; Xiong *et al.* 2018); see figure 10 for an illustration of type V shock interference produced by double wedge reflection.

The switch of the five triple points structure shown in figure 9(*b*) to type V shock interference is shown schematically in figure 11. The flow is measured in the reference frame co-moving with the intersection point P of shock I_S and shock S_{OR} (see figure 3*b*). The picture of the original flow structure shown in figure 11(*a*) is flipped upside down to become the picture shown in figure 11(*b*), which is further rotated in the clockwise direction to become the picture shown in figure 11(*c*).

The establishment of equivalence between the original problem and a shock interaction problem allows us to anticipate more shock reflection patterns for other sets of input parameters, as will be discussed in § 3.2. It is well-known that type V shock interference is caused by the interaction of two incident steady shock waves from the same family (Keyes & Hains 1973; Grasso *et al.* 2003). The switch of the observed shock reflection pattern of the present problem, as shown in figure 9(*b*), to the type V shock interference means that the RMS of the first family (I_s) and the initially steady-state shock wave (S_{OR}) constitute two incident shock waves of the same family when the reference frame co-moving with the intersection point P of I_S and S_{OR} is used.

It is also well-known that the interaction of two shock waves of the same family may also lead to type VI and type IV shock interference (Keyes & Hains 1973; Grasso *et al.* 2003). By switching between the original problem (present shock reflection with an RMS of the first family) and the equivalent problem (steady shock interaction problem), as illustrated in figure 12, we anticipate that the present shock reflection problem may produce a shock reflection pattern other than the type V shock reflection pattern, i.e. we may also have type VI and type IV shock reflection patterns as shown in figure 12(*a*). However, as we will see in § 3.4, the problem is even more complex than this.

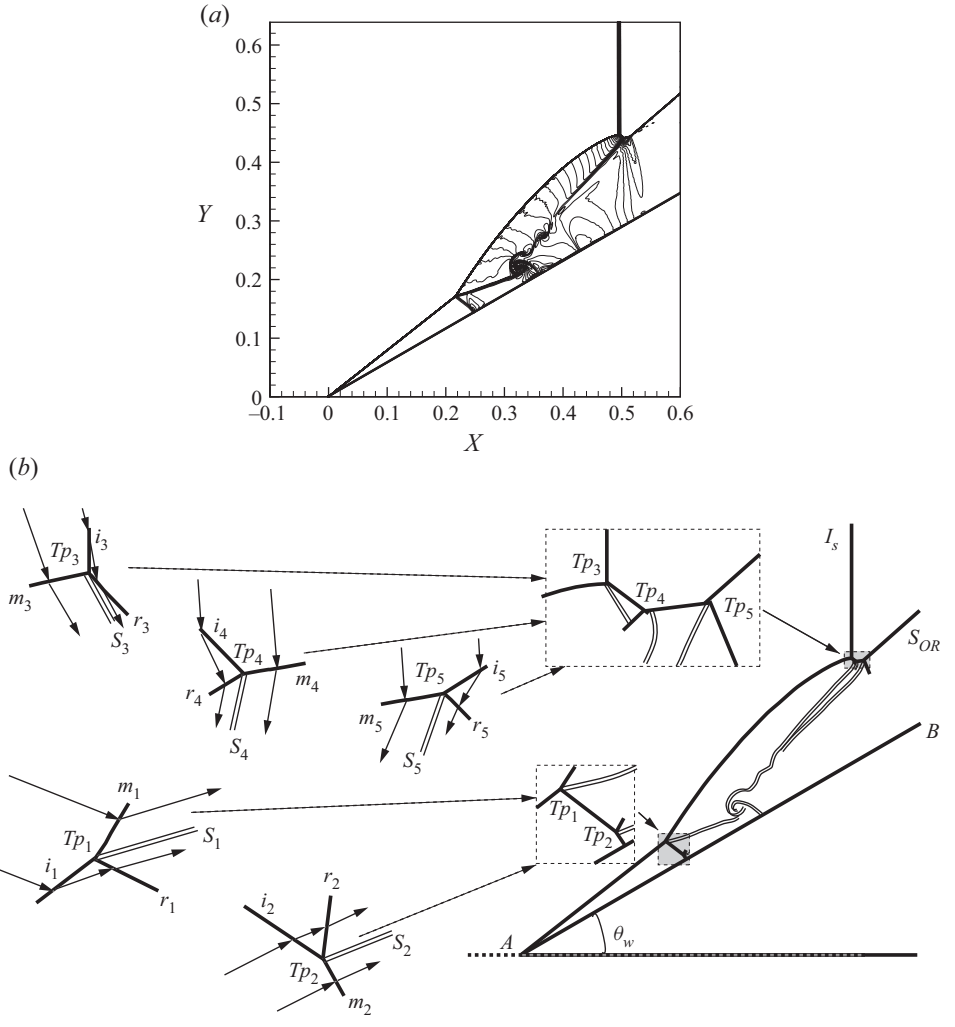

Figure 9. Shock reflection patterns: (*a*) Mach contours; (*b*) shock pattern.

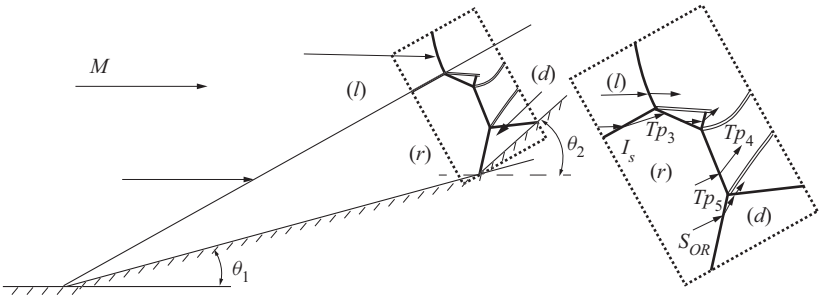

Figure 10. Schematic illustration of the double wedge reflection of type V.

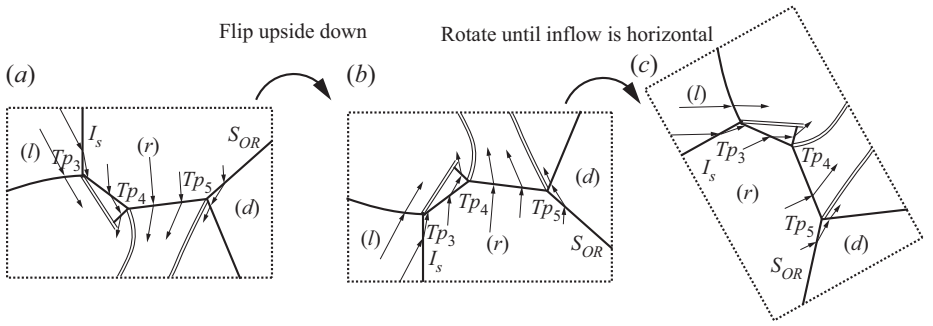

Figure 11. Schematic illustration of the procedure to switch to type V shock interference.

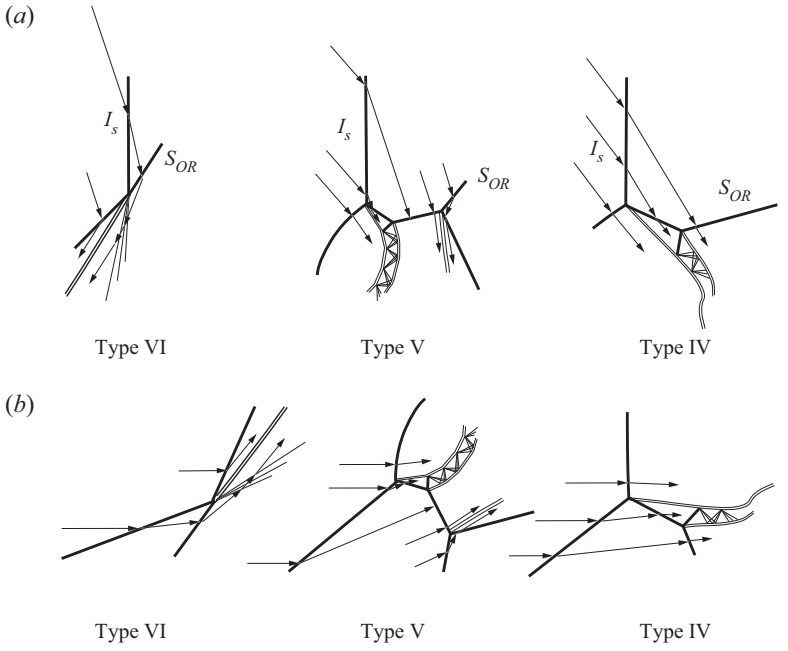

Figure 12. Correspondence between possible shock reflection patterns of the original problem (*a*) and possible shock interference patterns of the equivalent problem (*b*).

3.2. *Link of parameters between the original problem and the equivalent problem: flow deflection angle reversal*

To anticipate the shock reflection patterns of the original problem (reflection between the RMS and the SOSW with input parameters M_s, M_r and θ_w) using the knowledge of the equivalent problem (steady shock interaction between two incident shock waves with input parameters θ_1, θ_2 and M), we need to make a link between the input parameters of the present problem and those of the equivalent problem. The parameters used to establish such a link are labelled in figure 13. The link is obtained directly by using the frame co-moving with the intersection point P of I_S and S_{OR}. Here, θ_1 is the flow deflection angle across the first incident shock wave I_S (or the first wedge angle as shown in figure 10), and θ_2 is that across the second incident shock wave S_{OR} and measured with respect to the free-stream flow direction (or the second wedge angle as shown in figure 10).

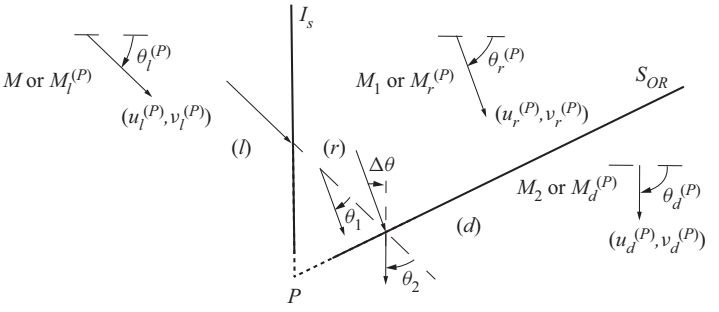

Figure 13. Flow parameters in the frame co-moving with the intersection point P of I_S and S_{OR} for an RMS of the first family. Only type V shock interference is considered.

The difference

$$\Delta\theta = \theta_2 - \theta_1 \tag{3.1}$$

measures the flow deflection angle across the shock wave S_{OR}. Now we provide the expressions for the link between θ_1, θ_2, M and M_s, M_r, θ_w. The parameters θ_1, θ_2, M follow from M_s, M_r, θ_w by switching flow parameters from the ground frame to the frame co-moving with the intersection point P.

On the ground frame, the Mach number M_d and speed of sound a_d in zone (d) (i.e. downstream of the steady shock wave S_{OR}) follow from the steady shock wave relation of S_{OR}. The flow velocities (u_d, v_d) of zone (d) in the ground frame are given by $u_d = M_d a_d \cos\theta_w$, $v_d = M_d a_d \sin\theta_w$. In regions (r) and (l), the velocities are $u_r = M_r a_r$ and $u_l = M_l a_l$, where M_r and M_l are given input flow parameters.

Now we derive the flow parameters in the frame co-moving with P. The superscript (P) is used to denote flow parameters in this co-moving frame. The velocity of the intersection point P of I_S and S_{OR} is given by (2.1). Thus the flow velocities of region (r), region (l) and region (d) in the co-moving frame are

$$\left.\begin{aligned}
(u_r^{(P)}, v_r^{(P)}) &= (u_r - u_P, -v_P) \quad \text{region } (r),\\
(u_l^{(P)}, v_l^{(P)}) &= (u_l - u_P, -v_P) \quad \text{region } (l),\\
(u_d^{(P)}, v_d^{(P)}) &= (u_d - u_P, v_d - v_P) \quad \text{region } (d).
\end{aligned}\right\} \tag{3.2}$$

Putting (3.2) into $M_l^{(P)} = \sqrt{(u_l^{(P)})^2 + (v_l^{(P)})^2}/a_l$ and $\theta_l^{(P)} = \arctan|v_l^{(P)}/u_l^{(P)}|$, and using the definition of the Mach number, we get the following expressions for the Mach number $M_l^{(P)}$ and flow deflection angle $\theta_l^{(P)}$ in region (l):

$$\left.\begin{aligned}
M_l^{(P)} &= \frac{\sqrt{(M_l a_l - M_s a_r)^2 + (M_s a_r \tan\beta_w)^2}}{a_l},\\
\theta_l^{(P)} &= \arctan\left(\left|\frac{M_s a_r \tan\beta_w}{M_l a_l - M_s a_r}\right|\right).
\end{aligned}\right\} \tag{3.3}$$

Putting (3.2) into $\theta_r^{(P)} = \arctan|v_r^{(P)}/u_r^{(P)}|$, we get the following expressions for the flow deflection angle $\theta_r^{(P)}$ in region (r):

$$\theta_r^{(P)} = \arctan\left(\left|\frac{M_s \tan\beta_w}{M_s - M_r}\right|\right). \tag{3.4}$$

The flow deflection angle $\theta_d^{(P)}$ in region (d) is then computed by

$$\theta_d^{(P)} = \begin{cases} \arctan\left|\dfrac{v_d^{(P)}}{u_d^{(P)}}\right|, & \text{if } u_d^{(P)} > 0,\ v_d^{(P)} < 0, \\ \pi - \arctan\left|\dfrac{v_d^{(P)}}{u_d^{(P)}}\right|, & \text{if } u_d^{(P)} < 0,\ v_d^{(P)} < 0, \\ \pi + \arctan\left|\dfrac{v_d^{(P)}}{u_d^{(P)}}\right|, & \text{if } u_d^{(P)} < 0,\ v_d^{(P)} > 0, \\ 2\pi - \arctan\left|\dfrac{v_d^{(P)}}{u_d^{(P)}}\right|, & \text{if } u_d^{(P)} > 0,\ v_d^{(P)} > 0. \end{cases} \tag{3.5}$$

The expression (3.2) is used to compute the right-hand sides of the above expressions.

The corresponding parameters θ_1, θ_2 and M in the equivalent problem, as shown in figure 13, can thus be expressed as

$$\left.\begin{aligned} \theta_1 &= \theta_r^{(P)} - \theta_l^{(P)}, \\ \theta_2 &= \theta_d^{(P)} - \theta_l^{(P)}, \\ M &= M_l^{(P)}. \end{aligned}\right\} \tag{3.6}$$

To identify the co-moving flow field, apart from parameters θ_1, θ_2 and M, the Mach number in the co-moving frame with point P in region (r) and region (d), denoted M_1 (or $M_r^{(P)}$) and M_2 (or $M_d^{(P)}$) are also needed. With the required flow velocity components given by (3.2), the Mach numbers M_1 (or $M_r^{(P)}$) and M_2 (or $M_d^{(P)}$) in the equivalent problem are obtained as

$$\left.\begin{aligned} M_1 = M_r^{(P)} &= \frac{\sqrt{(u_r^{(P)})^2 + (v_r^{(P)})^2}}{a_r}, \\ M_2 = M_d^{(P)} &= \frac{\sqrt{(u_d^{(P)})^2 + (v_d^{(P)})^2}}{a_d}. \end{aligned}\right\} \tag{3.7}$$

For a given set of M_s, M_r and θ_w, (3.6) provides the final set of relations to find the input parameters θ_1, θ_2 and M of the equivalent shock interaction problem, and (3.7) provides the final set of relations to find Mach numbers M_1 and M_2. Recall that we have defined $\Delta\theta = \theta_1 - \theta_2$, which can be regarded as the flow deflection angle of the second attached shock wave of the equivalent double wedge shock reflection.

For $M_r = 6$ and $M_s = 5.498$, the variations of θ_1, θ_2 and $\Delta\theta$ for $\theta_w \in [0^\circ, 40^\circ]$ are displayed in figure 14(*a*), and the variations of M, M_1 (or $M_r^{(P)}$) and M_2 (or $M_d^{(P)}$) for the same range of θ_w are displayed in figure 14(*b*). It is seen that, with increasing θ_w, the angle θ_1 decreases monotonically from 33.36° to 8.19°, and both M and M_1 increase monotonically. However, the curves for θ_2, $\Delta\theta = \theta_2 - \theta_1$ and M_2 are non-monotonic. For increasing θ_w, they first decrease, then increase, and finally decrease. The Mach number M_2 is smaller than M_1. When $\theta_w \to 0$, the SOSW is an infinitely weak oblique shock wave, and the flow parameters in region (r) are almost the same as those in region (d).

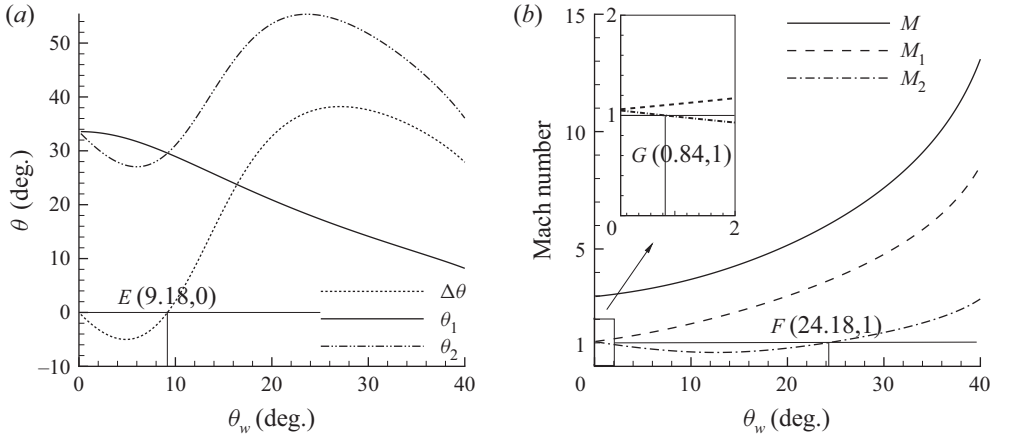

Figure 14. Variation of parameters with respect to θ_w for $M_r = 6$ and $M_s = 5.498$: (*a*) variation of θ_1, θ_2 and $\Delta\theta$; (*b*) variation of M, M_1 and M_2.

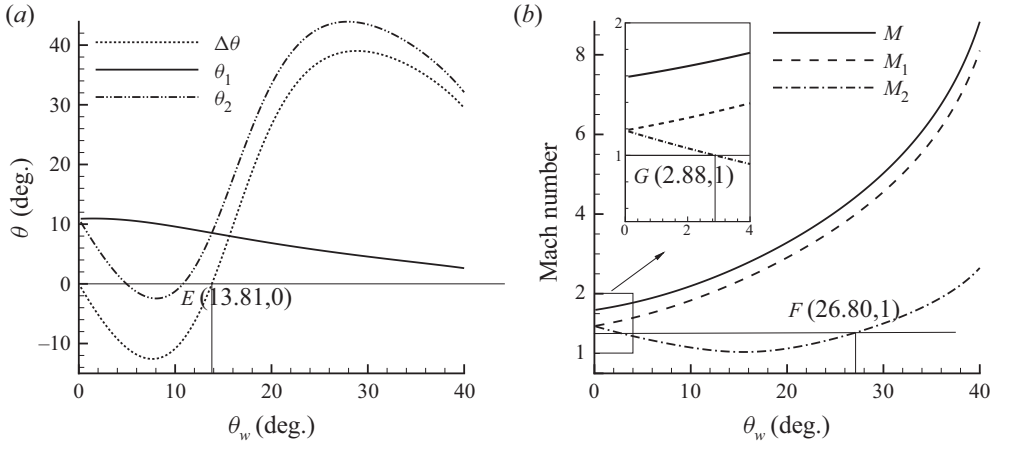

Figure 15. Variation of parameters with respect to θ_w for $M_r = 6$ and $M_s = 5.2$: (*a*) variation of θ_1, θ_2 and $\Delta\theta$; (*b*) variation of M, M_1 and M_2.

Two important phenomena are observed. The first is that M_2 is below 1 for $\theta_w \in [0^\circ, 24.18^\circ]$, and above 1 for $\theta_w \in [24.18^\circ, 40^\circ]$. This defines a condition that the incident shock wave S_{OR} becomes a strong one in the moving frame, which would be a condition for transition between types V and IV. In § 3.3, we indeed observe type IV shock interaction. The second phenomenon is that the difference $\Delta\theta$ is negative for $\theta_w \in [0^\circ, 9.18^\circ]$, while it is positive for $\theta_w \in [9.18^\circ, 40^\circ]$. This will be referred to *flow deflection angle reversal*, and this reversal will make the shock wave S_{OR} no longer an incident one but a reflected one, and type I and type II shock interference will occur; see § 3.4 for more details.

Similar phenomena are observed for other sets of conditions, as can be seen from figure 15 for $M_r = 6$ and $M_s = 5.2$.

3.3. *Discussion of the transition condition and possible shock reflection patterns*

The above correspondence of the present unsteady shock reflection problem to the equivalent shock interaction problem provides the input conditions θ_1, θ_2 and M for anticipating possible shock reflection patterns and for possible transition conditions.

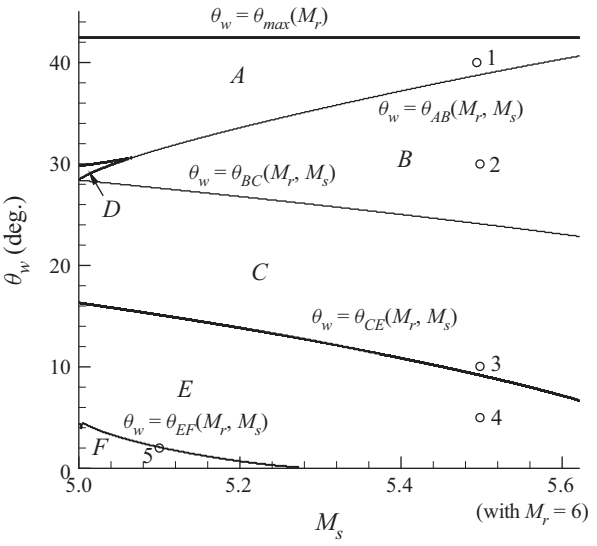

Figure 16. The six different domains in the M_s–θ_w plane with possible different shock reflection patterns for $M_r = 6$. The numbers 1, 2, 3, 4, 5 correspond to the test cases in table 1.

Conventional transition criteria for shock interaction. Transition conditions have been well studied for Edney's six types of shock interferences (Crawford 1973; Bramlette 1974; Grasso *et al.* 2003) and for the double wedge shock interaction problem (Olejniczak *et al.* 1997; Hu *et al.* 2010; Xiong *et al.* 2018). According to these studies, type VI and type V shock interactions may occur if a weak shock intersects another weak shock of the same family. The transition between type VI and type V shock interactions occurs when the merged shock wave reaches sonic condition behind it. Type IV and type III shock interferences occur when the downstream incident shock wave is a strong one. The transition between type V and type IV shock interference thus occurs when the downstream incident shock wave reaches sonic condition behind it. The transition between type III and type IV shock interference occurs when the slipline of the upper triple point intersects the wall at an angle beyond the detachment condition of the reflected shock wave. Type I and type II shock interferences occur when the two incident shock waves are weak and of different families, and transition between type I and type II occurs when the detachment of one reflected shock wave is reached. Note that if types VI, V and IV shock interferences are due to double wedge geometry, then more interference patterns are observed and the transition conditions are given by Olejniczak *et al.* (1997).

For any set of M_s, M_r and θ_w of the original problem, we compute θ_1, θ_2 and M for the equivalent shock interaction problem using the method in § 3.2. With θ_1, θ_2 and M thus obtained, we use the conventional transition criteria for shock interaction to build the transition conditions and draw these transition conditions back in the M_s–θ_w plane. The transition conditions thus obtained are displayed in figure 16 for $M_r = 6$. Note that, according to figure 5(*b*), the parameter range of M_s is $M_s \in [5.01, 5.62]$. The parameter range of θ_w is chosen to be $\theta_w \in [0^\circ, 45^\circ]$, which covers the detachment condition $\theta_w = \theta_{max}(M_r)$ of the steady oblique shock S_{OR}, computed by (2.5) (the situation with $\theta_w > \theta_{max}(M_r)$ is not considered in this paper).

Case	θ_w (deg.)	M_r	M_s	θ_1 (deg.)	$\Delta\theta$ (deg.)	M	M_1	M_2	Pressure ratio p_l/p_r
1	40	6	5.498	8.19	27.9	13.1	8.54	2.87	0.127
2	30	6	5.498	14.1	37.6	7.60	4.77	1.44	0.127
3	10	6	5.498	28.9	2.1	3.71	1.81	0.615	0.127
4	5	6	5.498	32.3	−5.01	3.26	1.38	0.775	0.127
5	2	6	5.1	5.11	−5.50	1.51	1.33	1.11	0.778

Table 1. Test cases for an RMS of the first family in figure 16. Here, θ_w, M_s and M_r are given, while θ_1, θ_2 and M are computed by (3.6), $\Delta\theta$ by (3.1), M_1, M_2 by (3.7), and p_l/p_r by (2.10).

Five cases are provided in table 1 and marked also in figure 16. These will be used for CFD computation to display the various shock reflection patterns that may appear in the regions of figure 16.

The six regions labelled A, B, C, D, E, F in figure 16 represent possible different shock reflection patterns. The shock polars at points 1, 2, 3 and some point inside region D are given in figures 17(a–d). According to transition analysis of the equivalent problem, region A should have type VI shock interference, region B should have type V shock interference, and region D should also have type VI shock interference but with the reflected expansion wave replaced by a shock wave (this is named type I by Olejniczak *et al.* (1997)). The line $\theta_w = \theta_{AB}(M_r, M_s)$ separates region (A,D) and region B. It is the condition that the merged shock wave (of the two incident shock waves of the equivalent problem) reaches the sonic condition. The line separating regions A and D is the condition that the reflected expansion fan of type VI shock interference begins to be replaced by a shock wave. Region C should have type IV shock interference. The line $\theta_w = \theta_{BC}(M_r, M_s)$, which separates regions B and C, is the sonic condition ($M_2 = 1$) of the equivalent problem for transition between type VI and type V shock interference, i.e. the downstream incident shock wave of the equivalent problem reaches the sonic condition.

The shock polar presentation of some types of reflections is shown in figure 17. Figures 17(a–c) correspond to cases 1–3, which are points 1–3 in figure 16. Figure 17(d) is the shock polar for some point in region D, for which $\theta_w = 29.577^\circ$, $M_r = 6$, $M_s = 5.017$, $M = 4.39$, $M_1 = 4.36$, $M_2 = 1.11$, $\theta_1 = 0.358^\circ$ and $\Delta\theta = 39.4^\circ$. Point ($n$), with $n = 1 - 8$, on the shock polar figures corresponds to region (n) illustrated in the subfigure inside the shock polar figure.

The line $\theta_w = \theta_{CE}(M_r, M_s)$, which separates region C from the regions below it, is due to flow deflection angle reversal (see § 3.2) and is of particular interest, so the discussion about it and the regions below it will be presented separately, in § 3.4. Due to this reversal, shock polars for regions E and F are provided separately in figure 18.

The numerical results for case 1, which lies in the type VI region of figure 16, are displayed in figure 19. We observe two incident shock waves, a merged shock wave, an expansion wave and a slipline, which is indeed type VI shock interference according to figure 12.

The numerical results for case 2, which lies in the type V region of figure 16, is indeed type V shock interference, according to the numerical results shown before in figure 9.

Case 3 lies in the type IV region of figure 16, and the numerical results are displayed in figure 20. An enlarged partial view of the Mach contours is given in figure 20(a). An enlarged partial view of pressure is displayed in figure 20(b). The global view of the

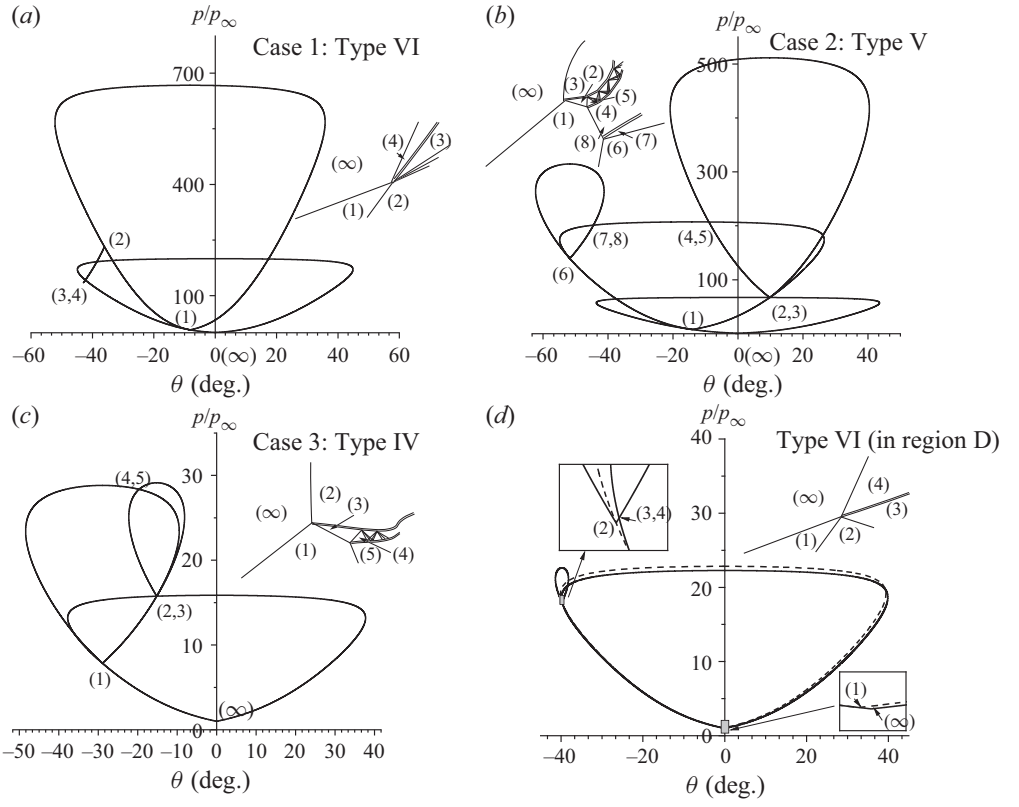

Figure 17. Shock polars of the equivalent problem: (*a*) case 1; (*b*) case 2; (*c*) case 3; (*d*) a point in region *D*.

pressure contours is displayed in figure 20(*c*). The streamlines marked in figure 20(*c*) are based in the frame co-moving with *P*. The structure is the same as type IV shock interference as displayed in figure 12: it has two incident shock waves, a Mach stem and a jet.

3.4. *Type I and type II shock interference due to flow deflection angle reversal*

The line $\theta_w = \theta_{CE}(M_r, M_s)$ in figure 16, which separates regions *C* and *E*, is of particular interest. This line corresponds to $\Delta\theta = 0$, where $\Delta\theta$, defined by (3.1), is the flow deflection angle across shock S_{OR}. Thus the line $\theta_w = \theta_{CE}(M_r, M_s)$ corresponds to the condition with flow deflection angle reversal discussed in § 3.2; see figure 14(*a*). Below this line, the shock S_{OR}, which is the downstream incident shock for type IV, V and VI shock interference when $\theta_w > \theta_{CE}(M_r, M_s)$, can no longer be regarded as an incident shock wave of the equivalent problem, but should be regarded as a reflected shock one. This means that the newly generated shock oblique shock wave S_{NE} (see figure 3*b*) should be one incident shock wave, apart from the RMS (I_S). The shock I_S and the shock S_{NE} then constitute two incident shock waves of different families, which should have type I and type II shock interaction (Keyes & Hains 1973; Grasso *et al.* 2003). The line $\theta_w = \theta_{EF}(M_r, M_s)$ in figure 16 is the transition condition between type I and type II shock interference. Region *E* above $\theta_w = \theta_{EF}(M_r, M_s)$ should have type II shock interference, and region *F* below $\theta_w = \theta_{EF}(M_r, M_s)$ should have type I shock interference.

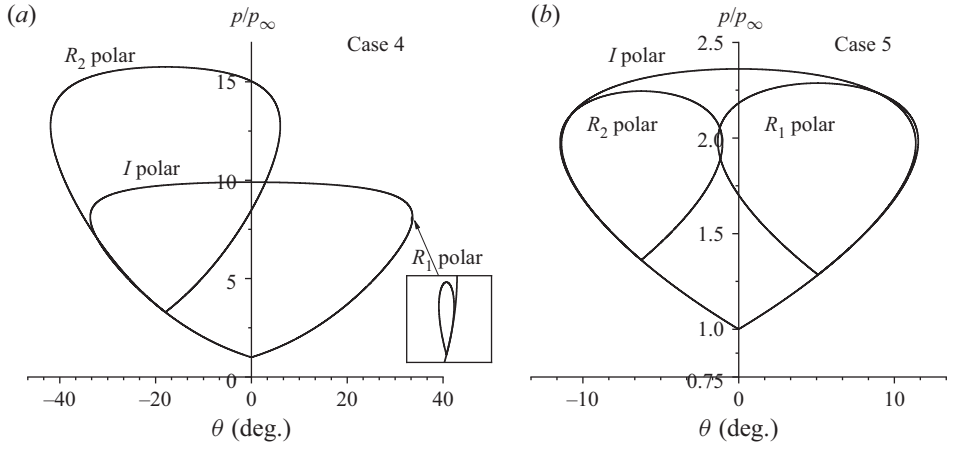

Figure 18. Shock polars for the asymmetric shock reflection problem (with deflection angle reversal for S_{NE} and I_S in figure 3): (*a*) case 4; (*b*) case 5.

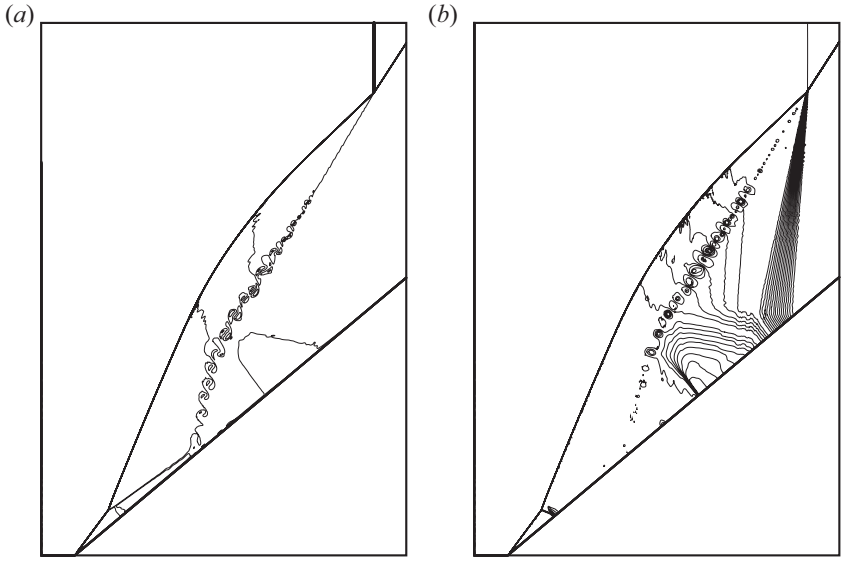

Figure 19. Type VI shock interaction for $\theta_w = 40^\circ$, $M_r = 6$, $M_s = 5.498$: (*a*) Mach contours; (*b*) pressure contours.

Case 4 in table 1 lies in region E, where we should have type II shock interference. The numerical solution for case 4 is displayed in figure 21, which is indeed type II shock interference. Figure 21(*a*) shows the Mach contours, figure 21(*b*) gives the pressure contours, and figure 21(*c*) shows the Mach contours and streamlines seen from the frame co-moving with the intersection point P. In this case, shock S_{OR} is one reflected shock of the type II shock interference, and shock I_S and the newly generated SOSW(S_{NE}) are the two incident shock waves according to the streamlines shown in figure 21(*c*). The shock S_{R2} is the other reflected shock wave.

Case 5 in table 1 lies in region F, where we should have type I shock interference. The numerical solution for case 5 is displayed in figure 22, which is indeed type I

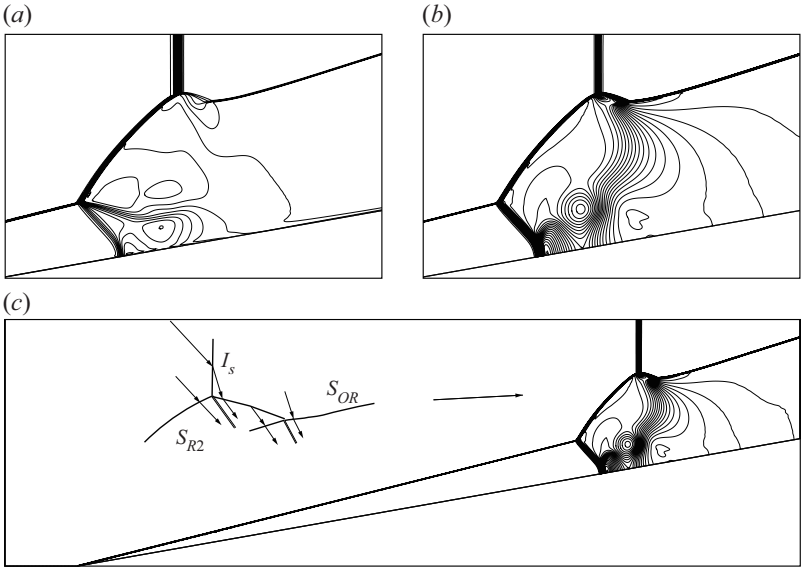

Figure 20. Type IV shock interaction for $\theta_w = 10^\circ$, $M_r = 6$, $M_s = 5.498$: (*a*) Mach contours; (*b*) pressure contours; (*c*) global view of pressure contours.

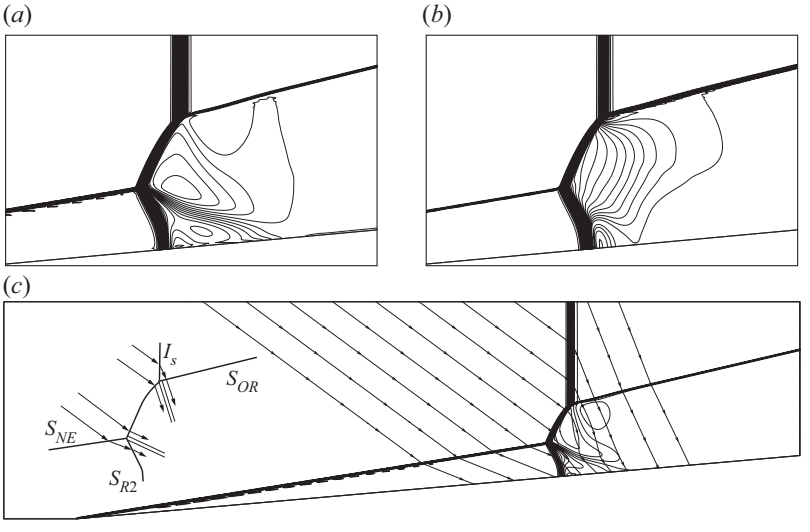

Figure 21. Type II shock interaction for $\theta_w = 5^\circ$, $M_r = 6$, $M_s = 5.498$: (*a*) Mach contours; (*b*) pressure contours; (*c*) Mach contours and streamlines in the co-moving frame.

shock interference. Figure 22(*a*) shows the Mach contours, figure 22(*b*) gives the pressure contours, and figure 22(*c*) shows the Mach contours and streamlines seen from the frame co-moving with the intersection point P of I_S and S_{OR}. In this case, shock S_{OR} is one reflected shock of the type I shock interference, and shock I_S and the newly generated SOSW(S_{NE}) are the two incident shock waves according to the streamlines shown in figure 22(*c*). The shock S_{R2} is the other reflected shock wave.

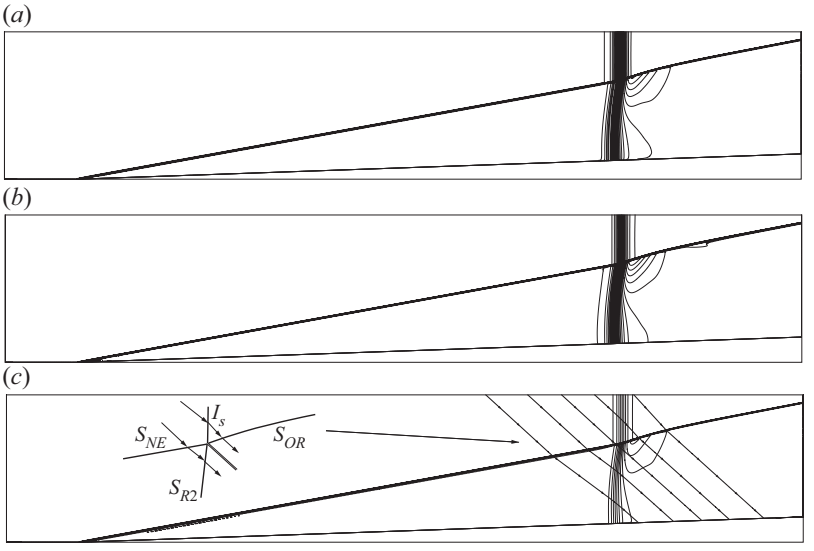

Figure 22. Type I shock interaction for $\theta_w = 2^\circ$, $M_r = 6$, $M_s = 5.498$: (*a*) Mach contours; (*b*) pressure contours; (*c*) Mach contours and streamlines in the co-moving frame.

Note that type I and type II shock interactions are called regular reflection and Mach reflection in asymmetric shock reflections (Li *et al.* 1999; Ivanov *et al.* 2002).

4. Reflection types and transition conditions for an RMS of the second family

This section is divided into five subsections, devoted respectively to display of some shock reflection patterns (using CFD) including the subdivision of the global reflection structure into primary and secondary reflection structures, the method for transition analysis of primary reflection, the method for transition analysis of secondary reflection, and the transition conditions for various shock reflection patterns.

4.1. *Some shock reflection patterns: primary and secondary reflections*

As noted in § 1, shock reflection for an RMS of the second family has been studied before within the context of shock-on-shock interaction. Li & Ben-Dor (1997) considered an oblique incident shock wave and derived analytical solutions for various shock reflection patterns. Law *et al.* (2003) performed some numerical simulation for shock-on-shock interaction, considering both oblique and normal incident shock waves. These studies have considered the influence of shock angle of the incident shock. Here, we study shock patterns and transition conditions for a normal shock, as for an RMS of the first family, with the emphasis on the role of shock speed. More subtypes of shock reflection patterns are expected to be found here.

Since the shock reflection patterns may be rather complex, it is convenient to consider the global reflection pattern to be a combination of primary reflection and secondary reflection. The primary reflection is the direct reflection at the intersection of the RMS (I_S) and the SOSW (S_{OR}). It may produce regular reflection (RR) and Mach reflection (MR). The secondary reflection is the reflection of reflected shock waves from primary reflection. It may also produce regular reflection and Mach reflection; the latter will be

Case	θ_w (deg.)	M_r	M_s	Pressure ratio p_l/p_r
1	15	5	30	729
2	30	5	30	729
3	42	8.2	10	3.61

Table 2. Test cases for an RMS of the second family. The parameters θ_w, M_s and M_r are specified. The pressure ratio p_l/p_r is computed by (2.10).

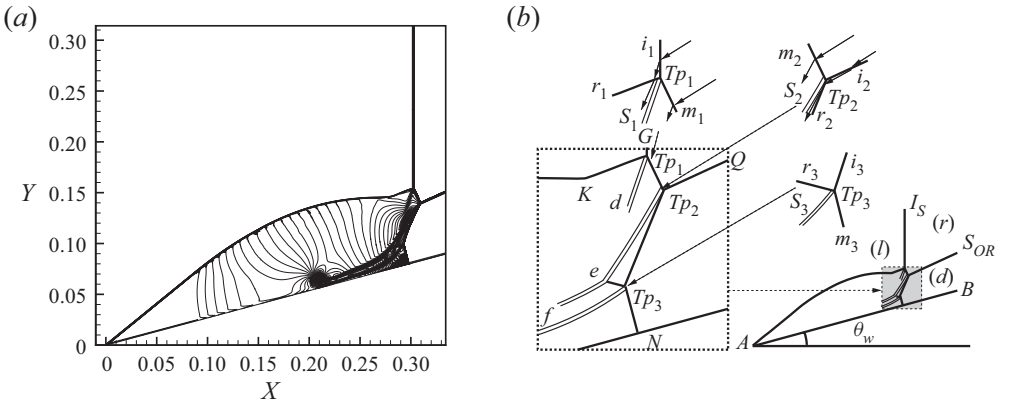

Figure 23. Shock reflection patterns for case 1: (*a*) Mach contours; (*b*) shock pattern.

called irregular reflection (IR) to follow the terminology in past studies of pseudo-steady reflection.

Three properly chosen test cases showing different primary shock reflection structures, with θ_w, M_s and M_r as given in table 2, are used for numerical simulation.

For case 1, the Mach contours at a typical instant are displayed in figure 23(*a*), and the reflection pattern, displaying the main flow structures and ignoring some details about interaction between shock waves and sliplines, is displayed in figure 23(*b*). The primary reflection, i.e. the direct reflection at the intersection of the RMS (I_S) and the SOSW (S_{OR}), is a Mach reflection, with Mach stem Tp_1Tp_2. The secondary reflection of the lower reflected shock wave, reflected from the triple point Tp_2, is an irregular reflection on the wedge, which produces another triple point Tp_3. There is a kink (K) on the reflected shock wave from triple point Tp_1.

For case 2, the Mach contours at a typical instant are displayed in figure 24(*a*), and the reflection pattern, with some details ignored, is displayed in figure 24(*b*). The primary reflection is a regular reflection. The secondary reflection of the lower reflected shock wave is an irregular reflection on the wedge, which produces another triple point Tp_3. There is an additional triple point Tp_4 on the reflected shock from triple point Tp_1.

For case 3, the Mach contours at a typical instant are displayed in figure 25(*a*) and the reflection pattern is displayed in figure 25(*b*). The primary reflection at point P is a regular reflection. The secondary reflection of the lower reflected shock wave produces a regular reflection at point R on the wedge. The reflected shock from point R further interacts with the slipline from the primary interaction point P, and this interaction produces a transmitted shock wave above that slipline. Similarly to case 2, there is an additional triple point Tp_4 on the reflected shock from the primary interaction point P. The reflected shock

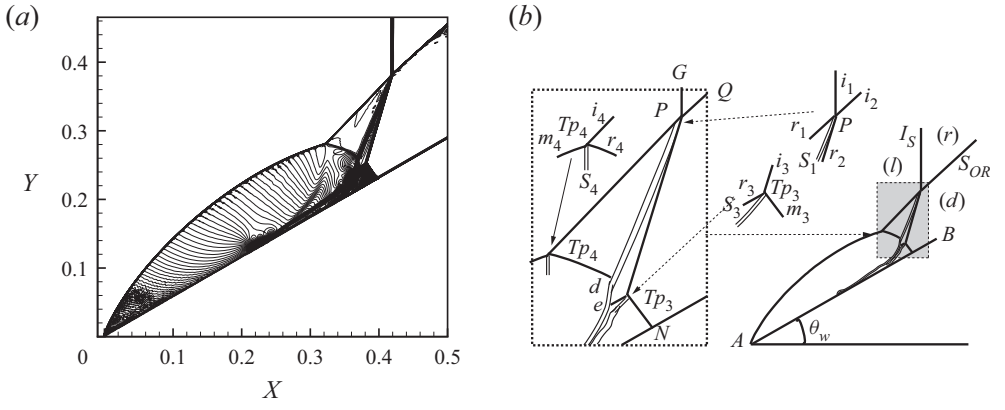

Figure 24. Shock reflection patterns for case 2: (*a*) Mach contours; (*b*) shock pattern.

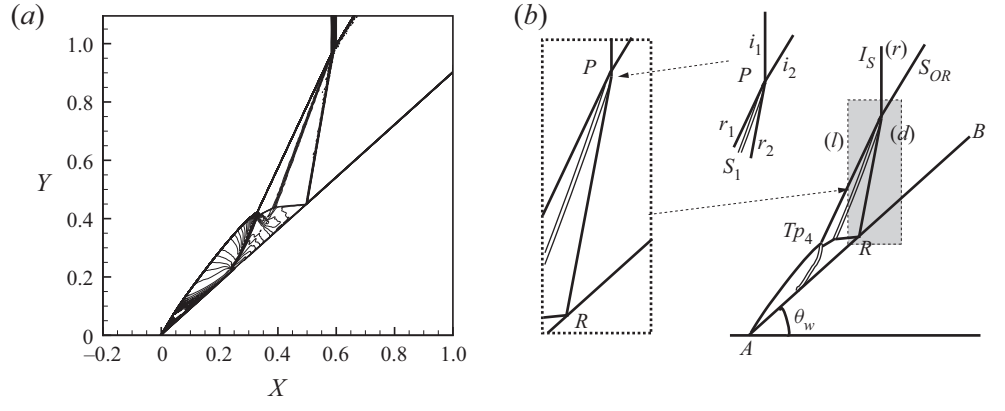

Figure 25. Shock reflection patterns for case 3: (*a*) Mach contours; (*b*) shock pattern.

from Tp_4 will interact with the transmitted shock from R. The full details are not displayed here since in this study we are concerned mainly with the primary and secondary reflection structures.

For an RMS of the second family, four possible primary–secondary reflection configurations, labelled RR-RR, RR-IR, MR-RR, MR-IR, are shown in figure 26. The RR-RR configuration (figure 26*a*) means that the RMS (I_S) and the SOSW (S_{OR}) have regular reflection at their direct intersection point (P), and the reflected shock (R_{S2}) of this reflection has regular reflection on the wall (at point R). The RR-IR configuration (figure 26*b*) means that the RMS (I_S) and the SOSW (S_{OR}) still have regular reflection at their direct intersection point (P) , and the reflected shock (R_{S2}) of this reflection has irregular reflection on the wall (with its Mach stem at point N on the wall). The MR-RR configuration (figure 26*c*) means that the RMS (I_S) and the SOSW (S_{OR}) have Mach reflection (with Mach stem Tp_1Tp_2), and the reflected shock (R_{S2}) of this reflection has regular reflection on the wall (at point R). The MR-IR configuration (figure 26*d*) means that the RMS (I_S) and the SOSW (S_{OR}) also have Mach reflection (with Mach stem Tp_1Tp_2) , and the reflected shock (R_{S2}) of this reflection has irregular reflection on the wall (with its Mach stem at point N on the wall). Types RR-RR and RR-IR have been predicted and found numerically before (cf. Li & Ben-Dor 1997; Law *et al.* 2003). The MR-RR

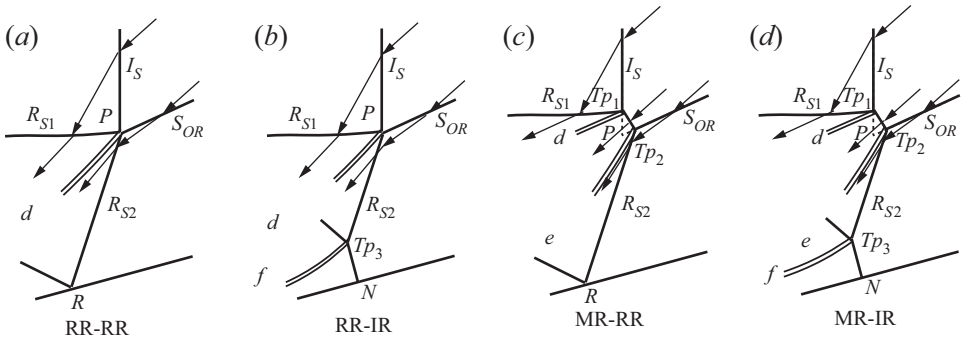

Figure 26. Possible flow patterns for an RMS of the second family. The reflection at the intersection point P is the primary reflection. The reflection of one reflected shock from primary reflection on the wedge is secondary reflection.

configuration is not observed in our numerical simulation, as will be further mentioned at the end of § 4.4. The MR-IR configuration shown in figure 23(*a*) is different from the case reported before. (Previous studies appear to have reported not an R_{S2} that further produces Mach reflection on the wall, but a curved R_{S2} directly connected to the wall, the condition for which will be studied in § 4.5.)

Apart from the secondary reflection of R_{S2} on the wall, the reflected shock R_{S1} may also have secondary reflection structure; see § 4.5 for further discussion.

4.2. *Method to find transition condition for primary reflection*

The primary reflection, i.e. reflection between I_S and S_{OR} at their intersection point (P), is an asymmetric reflection, and the reflection type can be decided in the frame co-moving with the intersection point P of I_S and S_{OR}, through looking for the von Neumann criterion and detachment criterion as by Li *et al.* (1999) and Ivanov *et al.* (2002) for steady asymmetric reflection. The flow parameters that need to be used for deriving the transition conditions are displayed in figure 27. We will use the superscript (P) for flow parameters in the frame co-moving with the intersection point P.

The flow velocity of region (0) in figure 27 is

$$(u_0^{(P)}, v_0^{(P)}) = (u_r - u_P, -v_P) = ((M_r - M_s)a_r, -M_s a_r \tan\beta_w), \tag{4.1}$$

where (u_P, v_P), the velocity of the intersection point P, is given by (2.1). Putting (4.1) into $M_0^{(P)} = \sqrt{(u_0^{(P)})^2 + (v_0^{(P)})^2}/a_r$ and $\theta_0^{(P)} = \arctan|v_0^{(P)}/u_0^{(P)}|$, and using (2.1), we get the following expressions for the Mach number and flow angle in region (0):

$$\left.\begin{aligned} M_0^{(P)} &= \sqrt{(M_r - M_s)^2 + (M_s \tan\beta_w)^2}, \\ \theta_0^{(P)} &= \arctan\left(\frac{M_s \tan\beta_w}{M_s - M_r}\right). \end{aligned}\right\} \tag{4.2}$$

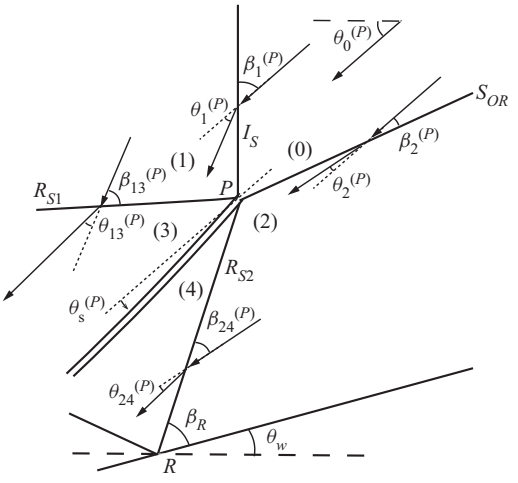

Figure 27. Schematic illustration of the asymmetric shock reflection in the co-moving frame with intersection point P (case RR-RR).

The shock angles $\beta_1^{(P)}$ and $\beta_2^{(P)}$ for the shocks I_S and S_{OR} in the frame co-moving with P are related to $(u_0^{(P)}, v_0^{(P)})$ by

$$\left.\begin{aligned} \beta_1^{(P)} &= \arccos\left(\frac{|v_0^{(P)}|}{|(u_0^{(P)}, v_0^{(P)})|}\right), \\ \beta_2^{(P)} &= \arccos\left(\frac{|u_0^{(P)}\cos\beta_w + v_0^{(P)}\sin\beta_w|}{|(u_0^{(P)}, v_0^{(P)})|}\right). \end{aligned}\right\} \tag{4.3}$$

The expressions (4.2) and (4.3) provide the input parameters $M_0^{(P)}$, $\theta_0^{(P)}$, $\beta_1^{(P)}$ and $\beta_2^{(P)}$ to be used for deriving the von Neumann condition and detachment condition using the method to find the transition condition of steady asymmetric reflection. In this paper, the shock waves I_S and S_{OR} are assumed to be weak shock waves viewing from the co-moving frame with point P. The case that they are strong shock waves is not considered.

The flow deflection angles $\theta_1^{(P)}$ and $\theta_2^{(P)}$ across the shocks I_S and S_{OR} shown in figure 27 are obtained from

$$\tan\theta_k^{(P)} = f_\theta(M_0^{(P)}, \beta_k^{(P)}), \quad k = 1, 2 \text{ (weak solution)}, \tag{4.4}$$

and the Mach number and pressure in regions (1) and (2) are computed as

$$(M_k^{(P)})^2 = f_M(M_0^{(P)}, \beta_k^{(P)}), \quad p_k^{(P)} = p_r f_p(M_0^{(P)}, \beta_k^{(P)}), \quad k = 1, 2. \tag{4.5}$$

Referring to figure 27 for notations for shock angles and flow deflection angles, the pressures $p_3^{(P)}$ and $p_4^{(P)}$ downstream of the reflected shock waves are computed by

$$\left.\begin{aligned} \tan\theta_{13}^{(P)} &= f_\theta(M_1^{(P)}, \beta_{13}^{(P)}), \quad p_3^{(P)} = p_1^{(P)} f_p(M_1^{(P)}, \beta_{13}^{(P)}), \\ \tan\theta_{24}^{(P)} &= f_\theta(M_2^{(P)}, \beta_{24}^{(P)}), \quad p_4^{(P)} = p_2^{(P)} f_p(M_2^{(P)}, \beta_{24}^{(P)}). \end{aligned}\right\} \tag{4.6}$$

The expressions in (4.6) are solved along with the flow parallel condition

$$\left.\begin{aligned}\theta_{13}^{(P)} &= \theta_1^{(P)} - \theta_s^{(P)},\\ \theta_{24}^{(P)} &= \theta_2^{(P)} + \theta_s^{(P)},\end{aligned}\right\} \tag{4.7}$$

and pressure balance condition

$$p_3^{(P)} = p_4^{(P)}. \tag{4.8}$$

In (4.7), $\theta_s^{(P)}$ is the slipline angle as shown in figure 27, and is assumed positive if it deflects in the anticlockwise direction relative to the direction of $(u_0^{(P)}, v_0^{(P)})$.

For given M_r and M_s, the detachment condition $\theta_w = \theta_w^{(D)}(M_r, M_s)$ is the condition of θ_w at which either $\theta_{13}^{(P)}$ reaches its detached angle or $\theta_{24}^{(P)}$ reaches its detached angle, i.e.

$$\theta_{13}^{(P)} = \theta_{max}(M_1^{(P)}) \quad \text{or} \quad \theta_{24}^{(P)} = \theta_{max}(M_2^{(P)}). \tag{4.9}$$

See (2.5) for the expression for the detached angle.

For given M_r and M_s, the von Neumann condition $\theta_w = \theta_w^{(N)}(M_r, M_s)$ is the condition of θ_w at which

$$p_m^{(P)} = p_3^{(P)} \quad \text{or} \quad p_m^{(P)} = p_4^{(P)}, \tag{4.10}$$

where the pressure $p_m^{(P)}$ downstream of a strong shock wave with flow deflection angle $\theta_s^{(P)}$ and with the upstream Mach number $M_0^{(P)}$ is calculated from

$$p_m^{(P)} = p_r\left(1 + \frac{2\gamma}{\gamma+1}\left(\left(M_0^{(P)}\sin\beta_s^{(P)}\right)^2 - 1\right)\right), \tag{4.11}$$

with $\beta_s^{(P)}$ being the strong shock wave solution of $\tan\theta_s^{(P)} = f_\theta(M_0^{(P)}, \beta_s^{(P)})$.

4.3. *Method for transition condition of secondary reflection of R_{S2}*

The secondary reflection, i.e. reflection of the reflected shock R_{S2} on the wedge, at point R as shown in figure 26, is a pseudo-steady reflection similar to that shown in figures 1(*c*,*d*). To find the transition condition of such a reflection, we need to know the velocity of R_{S2}. For RR-IR and RR-RR as shown in figure 26, this velocity can be found easily, and the transition condition will be considered in this subsection. For MR-IR and MR-RR in figure 26 this velocity can not be found easily.

Now consider pseudo-steady reflection of R_{S2} on the wedge. In a conventional study of pseudo-steady reflection, as shown in figures 1(*c*,*d*), the incident shock is in a vertical direction, i.e. the angle β_R displayed in figure 27 satisfies $\beta_R + \theta_w = 90^\circ$. Here it satisfies

$$\beta_R = \theta_0^{(P)} - \theta_2^{(P)} + \beta_{24}^{(P)} - \theta_w. \tag{4.12}$$

To find the transition condition, we need the speed V_R of the intersection point R between R_{S2} and the wedge surface. Note that R moves along the surface of the wedge. The flow

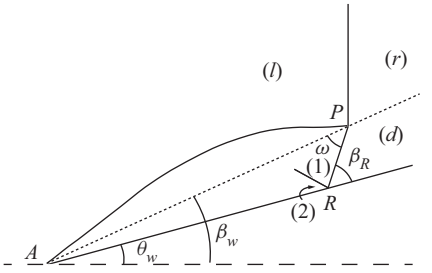

Figure 28. Flow parameters for determining the velocity of R.

parameters used for this are displayed schematically in figure 28, from which it can be seen that the following geometrical relation holds:

$$\frac{RA}{\sin\omega} = \frac{PA}{\sin\beta_R}, \tag{4.13}$$

with $\omega = \beta_R - (\beta_w - \theta_w)$. The speed of R is related to the speed V_P of point P by $V_R = V_P(RA/PA)$, where $V_P = M_s a_r/\cos(\beta_w)$ is the modulus of V_P already given by (2.1). Using (4.13) for RA/PA, we get

$$V_R = \frac{\sin(\beta_R - (\beta_w - \theta_w))}{\cos(\beta_w)\sin(\beta_R)} M_s a_r. \tag{4.14}$$

Now we use superscript (R) to denote flow parameters in the frame co-moving with R. The Mach number $M_d^{(R)}$ in region (d) is thus

$$M_d^{(R)} = \frac{V_R}{a_d} - M_d, \tag{4.15}$$

where M_d is the ground frame Mach number in region (d) calculated by $M_d^2 = f_M(M_r, \beta_w)$, and a_d is the sound speed in region (d) that follows from the sound speed expression and the oblique shock wave relation for density and pressure.

Now, with $M_d^{(R)}$ and β_R determined, the transition condition between RR and IR at point R can be decided as for pseudo-steady reflection. Out of various suggested criteria for the termination of RR, Ben-Dor (2006) pointed out that the one that best agrees with pseudo-steady shock tube experimental data is from the length scale concept of Hornung *et al.* (1979). This concept suggests that in pseudo-steady flows, RR terminates when the flow behind the reflection point, R, of the RR becomes sonic in a frame co-moving with R. With $M_k^{(R)}$ $(k = 1, 2)$ denoting the Mach number in region (k) $(k = 1, 2)$ of figure 28(a) in the frame co-moving with R, this criterion implies that the transition occurs when

$$M_2^{(R)} = 1, \tag{4.16}$$

where $M_2^{(R)}$ can be derived from the oblique shock wave relations

$$(M_2^{(R)})^2 = f_M(M_1^{(R)}, \beta_{12}^{(R)}), \tag{4.17}$$

where $M_1^{(R)}$ is calculated from $(M_1^{(R)})^2 = f_M(M_d^{(R)}, \beta_R)$, and $\beta_{12}^{(R)}$ is the weak solution of $\tan\theta_{d1}^{(P)} = f_\theta(M_1^{(R)}, \beta_{12}^{(R)})$, with $\theta_{d1}^{(P)}$ determined by $\tan\theta_{d1}^{(P)} = f_\theta(M_d^{(R)}, \beta_R)$.

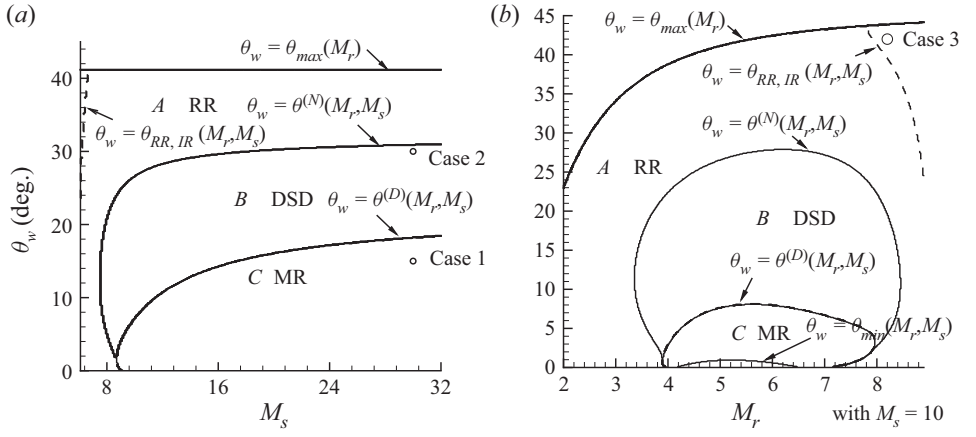

Figure 29. Transition criteria: (*a*) in the M_s–θ_w plane for $M_r = 5$; (*b*) in the M_r–θ_w plane for $M_s = 10$.

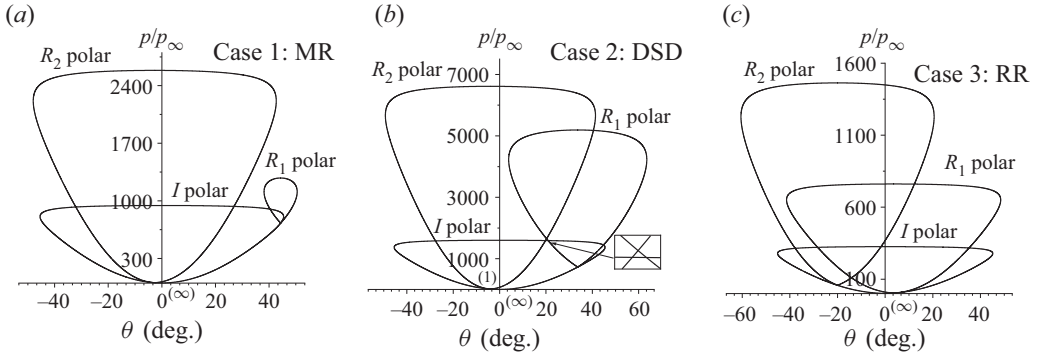

Figure 30. Shock polars for the primary reflection (in the frame co-moving with *P*): (*a*) case 1; (*b*) case 2; (*c*) case 3.

4.4. *Transition conditions in the $M_s - \theta_w$ and $M_r - \theta_w$ planes*

The transition conditions are expressed in either the M_s–θ_w plane for fixed M_r, or the M_r–θ_w plane for fixed M_s. The transition conditions in the M_s–θ_w plane for $M_r = 5$ are displayed in figure 29(*a*), and the transition conditions in the M_r–θ_w plane for $M_s = 10$ are displayed in figure 29(*b*). The shock polars for primary reflection in three cases (cases 1 and 2 shown in figure 29(*a*), and case 3 in figure 29(*b*) – see also table 2) are displayed in figure 30, with the *I* polar obtained from inflow Mach number $M_0^{(P)}$, and the R_1 and R_2 polars obtained from shock deflection angles $\theta_1^{(P)}$ and $\theta_2^{(P)}$.

In figure 29(*a*), the range of M_s is $M_s \in [6.1, 32]$. In figure 29(*b*), the range of M_r is $M_r \in [2, 8.9]$. This range is chosen from the requirement that $M_s > M_r + 1$ for an RMS of the second family.

Regions with RR, double solution (DSD) and MR shown in figure 29 are reflection types for primary reflection. Inside region *C* (Mach reflection), the line $\theta_w = \theta_{min}(M_r, M_s)$ is the critical angle to have one or more strong incident shock wave in the co-moving frame of the intersection point *P* of I_s and S_{OR}. The flow pattern below $\theta_w = \theta_{min}(M_r, M_s)$ will be discussed further in § 4.5. The dual solution domain is bounded below by the von

Neumann criterion $\theta_w = \theta_w^{(N)}(M_r, M_s)$ computed by (4.10), and bounded above by the detachment criterion $\theta_w = \theta_w^{(D)}(M_r, M_s)$ computed by (4.9). It is interesting to note that regular reflection occurs for large θ_w, while MR occurs for small θ_w, which appears to be counter-intuitive. A similar phenomenon is observed for an RMS of the first family, where type IV shock interference occurs at smaller θ_w while type VI shock interference occurs at larger θ_w.

The line $\theta_w = \theta_{RR,IR}(M_r, M_s)$ in figure 29 is the critical condition for transition of secondary reflection, i.e. for transition of the reflected shock wave R_{S2} over the wedge, in a region where the primary reflection is a regular reflection. On the left-hand side of $\theta_w = \theta_{RR,IR}(M_r, M_s)$, we have RR-IR. On the right-hand side of $\theta_w = \theta_{RR,IR}(M_r, M_s)$, we have RR-RR. In a region where the primary reflection is a Mach reflection, there is no simple way to obtain a similar transition criterion for the secondary reflection, since the velocity of the triple point Tp_2 is not known. As stated in § 4.1, the MR-RR configuration (figure 26*c*) did not appear in our numerical simulation. Since there is no simple way to derive the velocity of triple point Tp_2, no conclusion can be drawn about whether MR-RR is possible.

Now let us return to the shock polars displayed in figure 30. For case 1, the R_1 and R_2 polars have no intersection so the reflection type is MR. For case 2, the R_1 and R_2 polars have an intersection that is above the other two intersection points (the intersection point of the R_1 and I polars, and the intersection point of the R_2 and I polars), which means that case 2 is in the DSD domain. For case 3, the intersection point of the R_1 and R_2 polars is below the other two intersection points (the intersection point of the R_1 and I polars, and the intersection point of the R_2 and I polars), so the reflection type for case 3 is RR.

For another set of conditions, the results are similar. For instance, figure 31(*a*) presents the transition conditions in the M_r–θ_w plane with $M_s = 20$. It can be seen that the transition criteria are similar to those shown in figure 29(*b*) for $M_s = 10$. It is interesting to note that there is a non-monotonic variation for the detachment condition especially after $M_r \approx 17$. This non-monotonicity is made evident through displaying, in figure 31(*b*), the shock polars at points 1, 2 and 3 (with different M_r but with $\theta_w = 10.3^\circ$, $M_s = 20$) from figure 31(*a*). We observe MR for point 1, DSD for point 2, and MR again for point3.

The non-monotonicity might be due to the combined effects of the variations of the equivalent flow parameters ($M_0^{(p)}$, $\beta_1^{(P)}$ and $\beta_2^{(P)}$, computed by (4.2) and (4.3)) with respect to M_r, and these variations are shown in figure 32.

4.5. *Brief discussion of refection of secondary shock waves R_{S1} and R_{S2}*

The reflection of the secondary shock waves R_{S1} and R_{S2} shown in figure 26 may involve more patterns than discussed above. However, a complete study of all the possibilities is beyond the scope of this paper. Here we simply make an incomplete discussion.

4.5.1. *Reflection of the secondary shock wave R_{S1}*

In conventional pseudo-steady shock reflection, where a moving shock wave reflects over a wedge immersed initially in a still gas (as shown in figure 1*d*), the reflected shock wave (like R_{S1} here) in the case of Mach reflection may be smooth (a situation called single Mach reflection, SMR), have a kink (a situation called transitional Mach reflection, TMR), or have a new triple point (a situation called double Mach reflection, DMR); see figures 12 and 22 of Ben-Dor (2006) for more detailed classification of subtypes (such as direct,

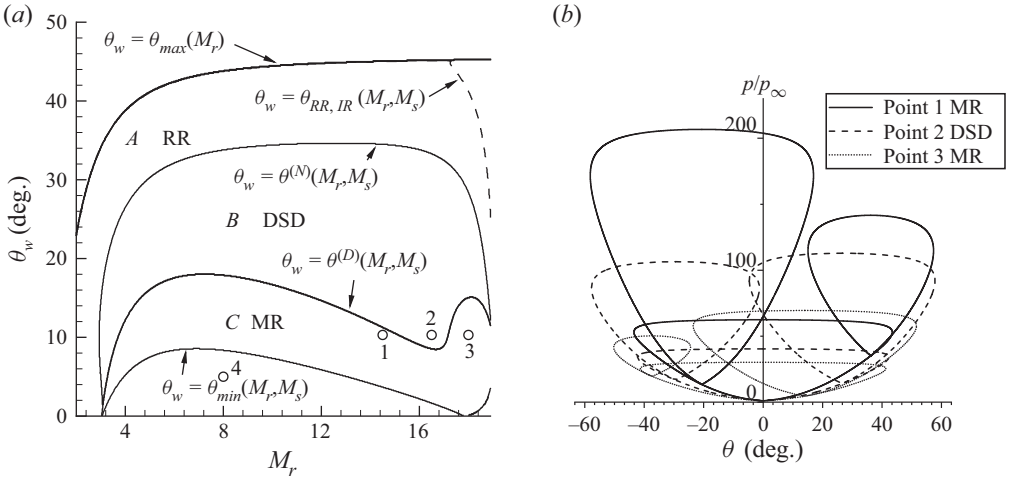

Figure 31. (*a*) Transition criteria for $M_s = 20$. (*b*) Shock polars (for points 1, 2 and 3).

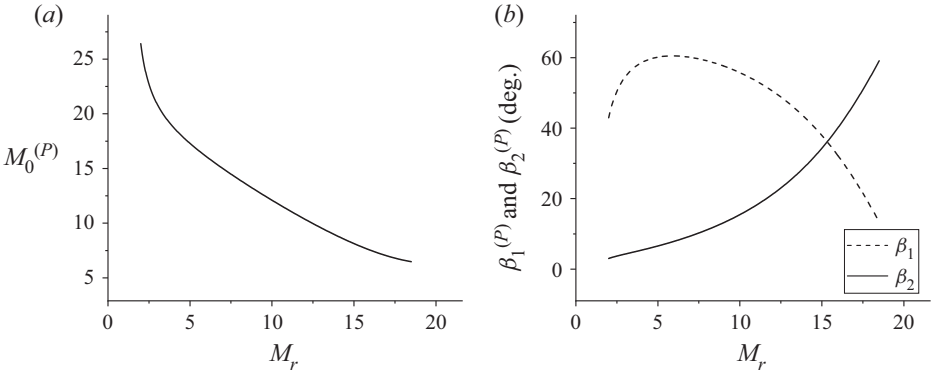

Figure 32. Dependence of some equivalent flow parameters on M_r for $M_s = 20$: (*a*) equivalent Mach number $M_0^{(P)}$; (*b*) equivalent shock angles $\beta_1^{(P)}$ and $\beta_2^{(P)}$.

stationary, inverse Mach reflections, DMR+, DMR−, or terminated RR) and transition conditions between various types of shock reflection.

It would be possible that for the present problem, the reflected shock wave R_{S1} from point Tp_1 of figure 23(*b*), or point *P* of figures 24(*b*) and 25(*b*), may also have a kink (point *K*) or an additional triple point. Indeed, in case 1 (MR-IR), we observe a kink according to figure 23(*a*), and this kink is marked *K* in figure 23(*b*). In this case, the primary reflection may be regarded as transitional Mach reflection. Previous studies (cf. Li & Ben-Dor 1997; Law *et al.* 2003) showed cases not with such a kink, but with a smooth R_{S1}. Now we also show a case with a smooth R_{S1}. This case has $M_s = 20$, $M_r = 8$, $\theta_w = 5^\circ$, corresponding to point 4 in figure 31(*a*), and this point is in the region below $\theta_w = \theta_{min}(M_r, M_s)$ (below which the incident shock is strong). The Mach contours and pressure contours for this condition are displayed in figures 33(*a*,*b*), respectively. In this case, R_{S1} is smooth and the primary reflection can be regarded as a single Mach reflection. However, we are unable to find a case for which the primary reflection (in the case of Mach reflection) is a double Mach reflection.

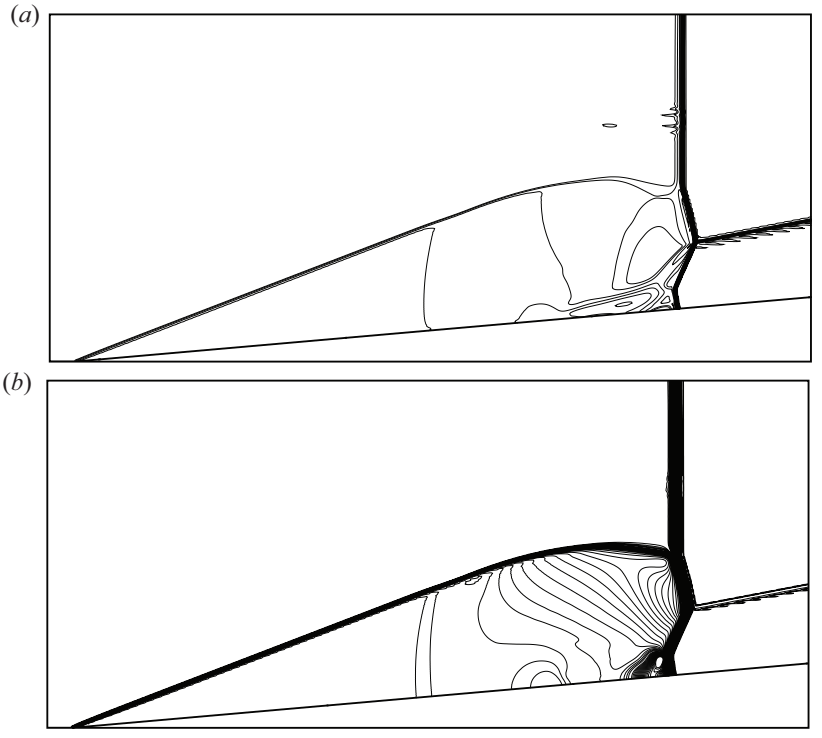

Figure 33. Shock reflection patterns for point 4 in figure 31(*a*) ($M_s = 20$, $M_r = 8$, $\theta_w = 5^\circ$): (*a*) Mach contours; (*b*) pressure contours.

The finding that we may have a smooth R_{S1} or a kink on R_{S1} raises the issue of determining further transition criteria to distinguish the conditions for SMR, TMR or possibly DMR for the present problem. Since TMR is observed above $\theta_w = \theta_{min}(M_r, M_s)$, and SMR is observed below, one may wonder whether $\theta_w = \theta_{min}(M_r, M_s)$ is the transition condition between SMR and TMR. However, this requires further study since transition conditions between SMR, TMR and DMR are far more complex than this even in the conventional pseudo-steady shock reflection problem, according to the studies by Li & Ben-Dor (1995) and Semenov *et al.* (2012).

In the conventional pseudo-steady shock reflection problem, the entire reflection process was treated as a combination of the shock-reflection process and the flow-deflection process (Li & Ben-Dor 1995). The transition condition between TMR and DMR requires knowledge of the velocity of the kink or the additional triple point, and simplified models, as given in the appendices of Li & Ben-Dor (1995), are already complex in the conventional pseudo-steady shock reflection case. If we follow the same approach, then the present problem is much more complicated since we need to know in addition the velocity of the triple point (Tp_1) of figures 26(*c*,*d*). Li & Ben-Dor (1997) provides a theory to estimate the velocity or trajectory in the equivalent shock-on-shock interaction problem. Thus, to derive transition conditions for various types of R_{S1} following the same approach as Li & Ben-Dor (1995) and Li & Ben-Dor (1997), one would have to combine the triple point trajectory theory of Li & Ben-Dor (1995) for a kink or a second triple point on R_{S1}, and the theory of Li & Ben-Dor (1997) for the triple point $Tp1$ shown in figures 26(*c*,*d*). It appears that such an analytical study would be highly complex, if not impossible, if one

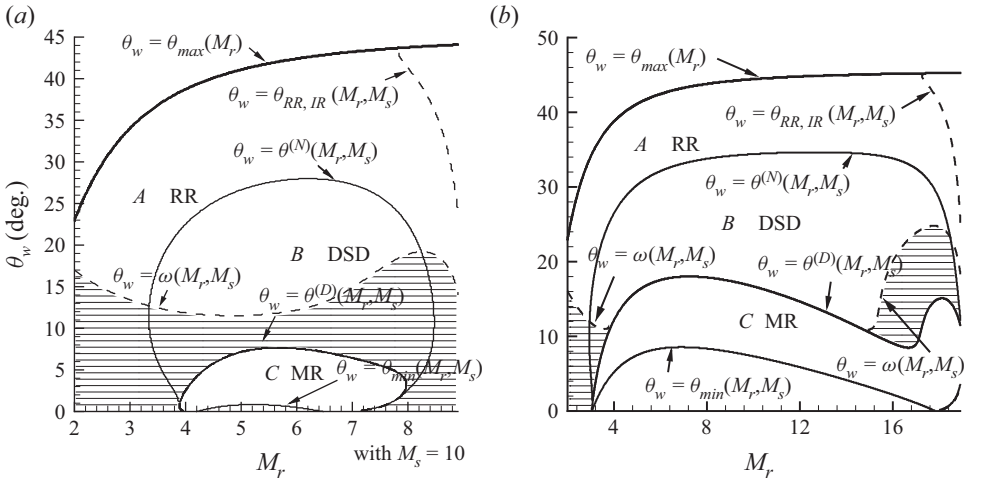

Figure 34. For primary reflection of RR, the region with R_{S2} being strong is displayed as the dashed region. Transition criteria in the M_r–θ_w plane for (*a*) $M_s = 10$, (*b*) $M_s = 20$.

wished to derive transition conditions for various possible types of R_{S1}, similar to that given in figure 10 of Li & Ben-Dor (1995) for the conventional pseudo-steady problem. Such a study will thus not be considered in the present paper, but may be considered in the future.

4.5.2. *Reflection of the secondary shock wave R_{S2} on the wall*

The reflection pattern of R_{S2} on the wall might also have more subtypes than shown in figure 26, if it were considered as the incident shock in the conventional pseudo-steady shock reflection problem. We immediately have the same difficulty as shown above for R_{S1} if one wants to investigate more details about the possible flow structure and the transition conditions, so such an issue is not considered in this study. We simply consider the subcase when R_{S1} becomes strong with respect to its reflection point on the wall.

The Mach contours displayed in figure 23(*a*) correspond to case 1 in figure 29(*a*), for which R_{S2} has Mach reflection, while the work of Li & Ben-Dor (1997) and Law *et al.* (2003) shows only a curved R_{S2}. Here we examine under which conditions this might occur.

In figure 26, R_{S2} is considered as a weak shock. In fact, R_{S2} may be also a strong shock wave seen from the reference frame attached to its intersection point on the wedge (point R of figure 26), according to the critical line $\theta_w = \omega(M_r, M_s)$ shown in figures 34(*a*,*b*) (which are obtained when the primary reflection is RR), which use the same conditions as figures 29(*b*) and 31(*a*). The critical line $\theta_w = \omega(M_r, M_s)$ is the condition above which R_{S2} is weak and below which R_{S2} is strong, in the frame co-moving with point R of figure 26. Shock reflection with R_{S2} strong happened to be computed by Law *et al.* (2003), who used a reference frame in which both shock waves are moving. Using the present frame (attached to the wedge), their cases in their figure 13(*a*,*c*) correspond to $M_s = 7.077$, $M_r = 4.431$, $\theta_w = 6^\circ$ (called case 1 here), and $M_s = 7.077$, $M_r = 4.431$, $\theta_w = 12^\circ$ (called case 2 here). These two cases will be used for comparison here.

For $M_s = 7.077$, the transition conditions, similar to those shown in figure 34, are displayed in figure 35(*a*). Figure 35(*b*) is the anticipated flow pattern. Cases 1 and 2 are

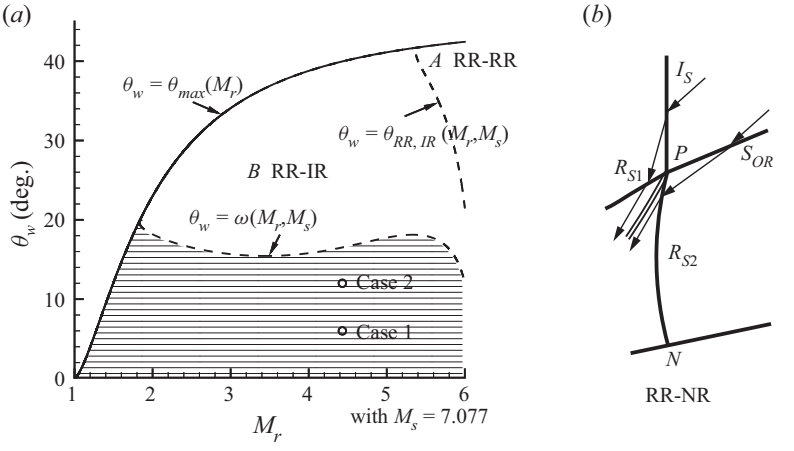

Figure 35. Shock reflection with strong R_{S2}: (*a*) transition criteria showing the critical line below which R_{S2} is strong (for $M_s = 7.077$); (*b*) hypothetical flow pattern (NR means no reflection).

shown as circles in figure 35(*a*). The mentioned two cases of Law *et al.* (2003) are indeed below the critical line $\theta_w = \omega(M_r, M_s)$, i.e. R_{S2} is strong in the reference frame co-moving with R.

The Mach contours for both cases computed here are displayed in figure 36(*a*,*b*). They compare well with numerical results of figure 13(*a*,*c*) of Law *et al.* (2003). The flow pattern in figure 36(*a*) is indeed similar to the anticipated flow pattern shown in figure 35(*b*).

Thus, at the condition well below the critical line $\theta_w = \omega(M_r, M_s)$, we recover the shock reflection part of previous studies, for which the reflected shock R_{S2} is a curved strong shock.

5. Conclusion

This paper addressed the reflection of a rightward moving shock (RMS) wave over a steady oblique shock wave (SOSW), the latter generated by a wedge immersed initially in a steady supersonic flow. Both families (the first and second families) are considered for the RMS wave. The shock patterns and transition conditions are studied.

For a rightward moving incident shock wave of the first family, we used a transformation to show that for a sufficiently large wedge angle, the original shock reflection problem can be switched to an equivalent steady shock interaction problem where the RMS and the right part of the SOSW are the two incident shock waves of the same family. Thus type VI, V, IV shock interactions may occur.

For a rightward moving incident shock wave of the first family reflecting over the steady shock produced by a wedge with a small wedge angle, a flow deflection angle reversal is observed, and the right part of the SOSW can no longer be regarded as one incident shock wave. Now the left part of the SOSW becomes one incident shock wave. This situation produces type I or type II shock interference.

For a rightward moving incident shock wave of the second family, studied previously within the context of shock-on-shock interaction, we decomposed the reflection into a combination of primary reflection (between the RMS and the SOSW) and secondary reflection (reflection of the reflected shock waves from primary reflection) and identified the transition conditions in the shock speed–wedge angle plane for major

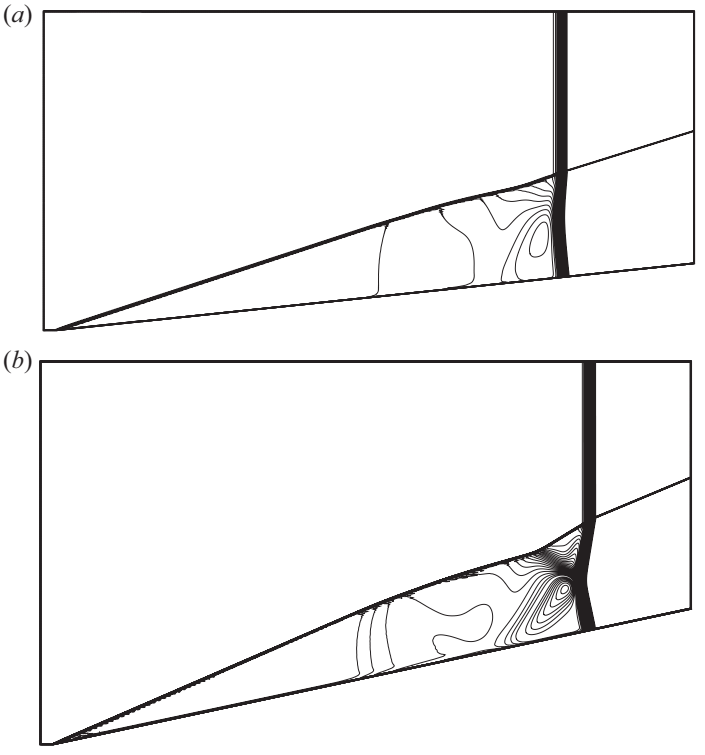

Figure 36. (*a*) Mach contours for case 1 ($M_s = 7.077$, $M_r = 4.431$, $\theta_w = 6^\circ$). (*b*) Mach contours for case 2 ($M_s = 7.077$, $M_r = 4.431$, $\theta_w = 12^\circ$).

reflection phenomena. For secondary reflection, one reflected shock wave impinges the wall to create regular reflection (RR) or irregular reflection (IR), and the other reflected shock wave is similar to the reflected wave of the classic pseudo-steady shock reflection (i.e. pseudo-steady shock reflection by a moving shock wave off a wedge immersed initially in a still gas). This other reflected shock wave may be smooth, or have a kink or another triple point similar to single Mach reflection, transitional Mach reflection and double Mach reflection observed from the classical pseudo-steady shock reflection. Hence there are quite a number of combinations of shock reflection patterns, more than predicted before in shock-on-shock interaction studies. However, the critical conditions for transition between various possible shock patterns of secondary reflected shock waves need more study in the future.

The large number of shock reflection patterns and the complexity of transition between various reflection patterns revealed in this study for reflection of RMSs of the two families on an SOSW enrich our knowledge of shock reflection or shock interaction. In this paper, we mainly considered the primary reflection patterns and their transition conditions, with some details about the secondary reflection not fully considered. These details may be considered in future studies.

Acknowledgement. The authors wish to thank the Referees, whose comments and suggestions were very useful for improving the paper.

Funding. This work was supported partly by the National Key Project (Grant no. GJXM92579) and by the National Science and Technology Major Project 2017-II-003-0015.

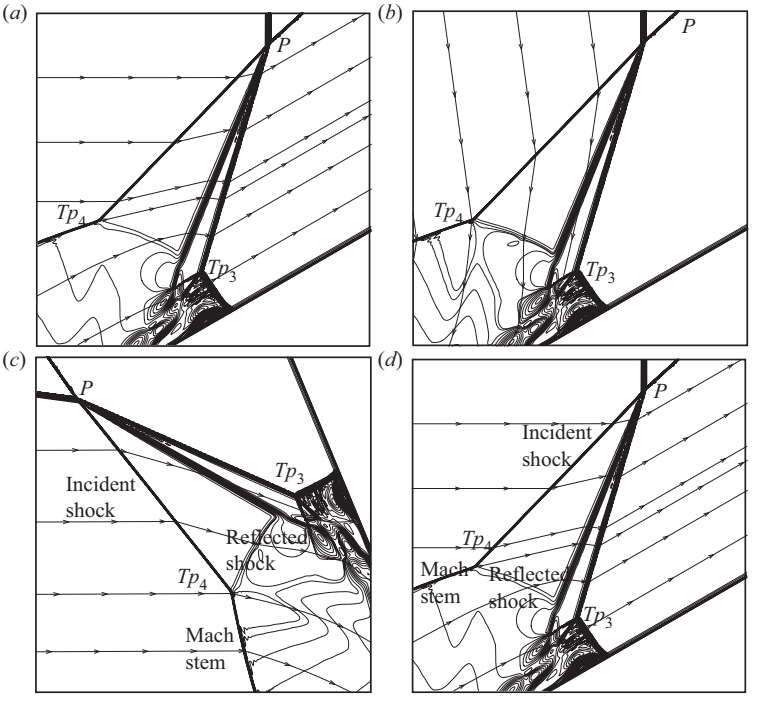

Figure 37. Illustration of identification of the shock structure of a moving triple point. (*a*) Original ground frame solution near triple point Tp_4. (*b*) Solution in the frame co-moving with the triple point Tp_4. (*c*) Numerical solution in the rotated frame. (*d*) Flow structure with the incident shock, reflected shock and Mach stem pertinent to triple point Tp_4 identified in the original ground frame.

Declaration of interests. The authors report no conflict of interest.

Author ORCIDs.
Zi-Niu Wu https://orcid.org/0000-0002-4405-0865.

Appendix. Triple point structure identification (TPSI) method

When CFD gives numerical results from which one perceives a number of moving triple points, it is difficult to determine which shock waves are the incident one, reflected one and Mach stem, as illustrated in figure 8 for steady flow. The TPSI method proposed by Wang & Wu (2021) makes it easier to identify the nature of various shock waves connected to a numerically computed moving triple point.

The method is, in fact, simple. Pick up the velocity of the triple point, say $\boldsymbol{V}_{TP}$, from numerical solutions at two different instants. The original flow velocity $\boldsymbol{V}$ by numerical computation is then subtracted from $\boldsymbol{V}_{TP}$ to get $\boldsymbol{V}^{(TP)} = \boldsymbol{V} - \boldsymbol{V}_{TP}$. We then use $\boldsymbol{V}^{(TP)}$ to draw the streamlines and Mach contours. This gives the streamlines and Mach contours in the frame co-moving with the triple point. We then rotate the frame in such a way that the local inflow streamlines are horizontal, until the flow structure is comparable to that shown in figure 8 and from which it is clear which shock waves are the incident one, reflected one and Mach stem.

Consider the triple point Tp_4 in figure 24(*b*) (case 2 in table 2). Figure 37(*a*) displays the Mach contours and streamlines in the ground frame. Using the numerical results, we

measured $V_{Tp4} = (23a_r, 20.2a_r)$. Figure 37($b$) displays the Mach contours and streamlines in the frame co-moving with the triple point, i.e. using $V^{(TP)} = V - V_{TP}$.

Figure 37(c) shows the results by rotation of figure 37(b) in such a way the inflow is horizontal. It is then clear from figure 37(c) which shocks are the incident one, reflected one and Mach stem, now marked in figure 37(c).

By correspondence between figures 37(a) and 37(c), the nature of shock waves pertinent to triple point Tp_4 is identified, as shown now in figure 37(d), which gives the flow structure in the original ground frame.

Here we showed the details of determining only an upward triple point. The method is similar for a downward triple point.

References

Athira, C.M., Rajesh, G., Mohanan, S. & Parthasarathy, A. 2020 Flow interactions on supersonic projectiles in transitional ballistic regimes. *J. Fluid Mech.* **894**, A27.

Ben-Dor, G. 1988 Steady, pseudo-steady and unsteady shock wave reflections. *Prog. Aerosp. Sci.* **25**, 329–412.

Ben-Dor, G. 2006 A state-of-the-knowledge review on pseudo-steady shock-wave reflections and their transition criteria. *Shock Waves* **15**, 277–294.

Ben-Dor, G. 2007 *Shock Wave Reflection Phenomena*. Springer. (Imprint: Springer).

Ben-Dor, G., Igra, O., Elperin, T. & Lifshitz, A. 2001 *Handbook of Shock Waves*. Academic Press.

Ben-Dor, G., Ivanov, M., Vasilev, E.I. & Elperin, T. 2002 Hysteresis processes in the regular reflection 2 Mach reflection transition in steady flows. *Prog. Aerosp. Sci.* **38**, 347–387.

Bramlette, T. 1974 Simple technique for predicting type III and IV shock interference. *AIAA J.* **12**, 1151–1152.

Chpoun, A., Passerel, D., Li, H. & Ben-Dor, G. 1995 Reconsideration of the oblique shock wave reflection in steady flows. Part 1. Experimental investigation. *J. Fluid Mech.* **301**, 19–35.

Crawford, D.H. 1973 A graphical method for the investigation of shock interference phenomena. *AIAA J.* **11**, 1590–1592.

Edney, B. 1968 Anomalous heat transfer and pressure distributions on blunt bodies at hypersonic speeds in the presence of an impinging shock. *Tech Rep*. 115. The Aerospace Research Institute of Sweden.

Frame, M.J. & Lewis, M.J. 1997 Analytical solution of the type IV shock interaction. *J. Propul. Power* **13**, 601–609.

Grasso, F., Purpura, C.B. & Délery, J. 2003 Type III and type IV shock/shock interferences: theoretical and experimental aspects. *Aerosp. Sci. Technol.* **7**, 93–106.

Henderson, L.F. & Lozzi, A. 1975 Experiments on transition of Mach reflection. *J. Fluid Mech.* **68**, 139–155.

Hornung, H.G. 2014 Mach reflection in steady flow. I. Mikhail Ivanov s contributions, II. Caltech stability experiments. *AIP Conf. Proc.* **1628**, 1384–1393.

Hornung, H.G., Oertel, H. & Sandeman, R.J. 1979 Transition to Mach reflection of shock waves in steady and pseudo-steady flows with and without relaxation. *J. Fluid Mech.* **90**, 541–560.

Hu, Z.M., Gao, Y.L., Myong, R.S., Dou, H.S. & Khoo, B.C. 2010 Geometric criterion for RR↔MR transition in hypersonic double-wedge flows. *Phys. Fluids* **22**, 016101.

Ivanov, M.S., Ben-Dor, G., Elperin, T., Kudryavtsev, A. & Khotyanovsky, D. 2001 Flow-Mach-number-variation-induced hysteresis in steady flow shock wave reflections. *AIAA J.* **39**, 972–974.

Ivanov, M.S., Ben-Dor, G., Elperin, T., Kudryavtsev, A.N. & Khotyanovsky, D.V. 2002 The reflection of asymmetric shock waves in steady flows: a numerical investigation. *J. Fluid Mech.* **469**, 71–87.

Keyes, J.W. & Hains, F.D. 1973 Analytical and experimental studies of shock interference heating in hypersonic flows, NASA TN D-7139.

Klopfer, G.H., Yee, H.C. & Kutler, P. 1989 Numerical study of unsteady viscous hypersonic blunt body flows with an impinging shock. In *11th International Conference on Numerical Methods in Fluid Dynamics* (ed. by D.L. Dwoyer, M.Y. Hussaini & R.G. Voigt), pp. 337–343. Springer.

Kudryavtsev, A.N., Khotyanovsky, D.V., Ivanov, M.S., Hadjadj, A. & Vandromme, D. 2002 Numerical investigations of transition between regular and Mach reflections caused by free-stream disturbances. *Shock Waves* **12**, 157–165.

KUTLER, P., SAKELL, L. & AIELLO, G. 1975 Two-dimensional shock-on-shock inter action problem. *AIAA J.* **13** (3), 361–367.

LAW, C., FELTHUN, L.T. & SKEWS, B.W. 2003 Two-dimensional numerical study of planar shock-wave/moving-body interactions. *Shock Waves* **13** (5), 381–394.

LI, H. & BEN-DOR, G. 1995 Reconsideration of pseudo-steady shock wave reflections and the transition criteria between them. *Shock Waves* **5**, 59–73.

LI, H. & BEN-DOR, G. 1996 Application of the principle of minimum entropy production to shock wave reflections. I. Steady flows. *J. Appl. Phys.* **80**, 2027–2037.

LI, H. & BEN-DOR, G. 1997 Analytical investigation of two-dimensional unsteady shock-on-shock interactions. *J. Fluid Mech.* **340**, 101–128.

LI, H., CHPOUN, A. & BEN-DOR, G. 1999 Analytical and experimental investigations of the reflection of asymmetric shock waves in steady flow. *J. Fluid Mech.* **390**, 25–43.

LIU, M.S. 1996 A sequel to AUSM: AUSM+. *J. Comput. Phys.* **129**, 364–382.

VON NEUMANN, J. 1943 Oblique reflection of shock. *Explos. Res. Rep.* 12. Navy Dept., Bureau of Ordinance, Washington, DC.

VON NEUMANN, J. 1945 Refraction, intersection and reflection of shock waves. *NAVORD Rep. 203–245*, Navy Dept., Bureau of Ordinance, Washington, DC.

OLEJNICZAK, J., WRIGHT, W.J. & CANDLER, G.V. 1997 Numerical study of inviscid shock interactions on double-wedge geometries. *J. Fluid Mech.* **352**, 1–25.

SEMENOV, A.N., BEREZKINA, M.K. & KRASSOVSKAYA, I.V. 2012 Classification of pseudo-steady shock wave reflection types. *Shock Waves* **22**, 307–316.

SMYRL, J.L. 2006 The impact of a shock-wave on a thin two-dimensional aerofoil moving at supersonic speed. *J. Fluid Mech.* **15**, 223–240.

TESHUKOV, V.M. 1989 On stability of RR of shock waves. *Zh. Prikl. Mekh. Tekh. Fiz.* **2**, 26–33.

VUILLON, J., ZEITOUN, D. & BEN-DOR, G. 1995 Reconstruction of oblique shock wave reflection in steady flows. Part 2. Numerical investigation. *J. Fluid Mech.* **301**, 37–50.

WANG, M.M. & WU, Z.N. 2021 Reflection of a moving shock wave over an oblique shock wave. *Chin. J. Aeronaut.* **34**, 399–403.

WINDISCH, C., REINARTZ, B.U. & MULER, S. 2016 Investigation of unsteady Edney type IV and VII shock–shock interactions. *AIAA J.* **54**, 1846–1861.

XIONG, W., LI, J., ZHU, Y. & LUO, X. 2018 RR–MR transition of a type V shock interaction in inviscid double-wedge flow with high-temperature gas effects. *Shock Waves* **28**, 751–763.